Quark contributions to baryon magnetic moments in full, quenched, and partially quenched QCD

Derek B. Leinweber*
Department of Physics and Mathematical Physics and Special Research Centre for the Subatomic Structure of Matter, University of Adelaide 5005, Australia
(Received 13 November 2002; published 23 January 2004)

The chiral nonanalytic behavior of quark-flavor contributions to the magnetic moments of octet baryons is determined in full, quenched and partially quenched QCD, using an intuitive and efficient diagrammatic formulation of quenched and partially quenched chiral perturbation theory. The technique provides a separation of quark-sector magnetic-moment contributions into direct sea-quark loop, valence-quark, indirect sea-quark loop and quenched valence contributions, the latter being the conventional view of the quenched approximation. Both meson and baryon mass violations of $SU(3)$-flavor symmetry are accounted for. Following a comprehensive examination of the individual quark-sector contributions to octet baryon magnetic moments, numerous opportunities to observe and test the underlying structure of baryons and the nature of chiral nonanalytic behavior in QCD and its quenched variants are discussed. In particular, the valence u-quark contribution to the proton magnetic moment provides the optimal opportunity to directly view nonanalytic behavior associated with the meson cloud of full QCD and the quenched meson cloud of quenched QCD. The u quark in Σ^+ provides the best opportunity to display the artifacts of the quenched approximation.

DOI: 10.1103/PhysRevD.69.014005 PACS number(s): 12.39.Fe, 12.38.Gc, 13.40.Em

I. INTRODUCTION

One of the grand promises of lattice-regularized QCD is to provide *ab initio* predictions of hadronic observables with statistical and systematic uncertainties constrained to within 1%. To realize this goal, extrapolations are required. The finite lattice spacing must be extrapolated to the continuum limit. The impact of the finite volume of the periodic lattice must be understood and extrapolated to infinity. For computational reasons, the masses of the light u and d quarks must be extrapolated from rather large values to the point at which the physical hadron masses are reproduced.

The realization of chiral symmetry in the dynamically broken Goldstone mode induces important nonanalytic behavior in hadronic observables as a function of quark mass. This makes extrapolations of hadronic observables highly nontrivial [1–15]. Significant curvature is encountered as one approaches the chiral limit. Indeed there is some controversy on the optimal methodology for achieving systematic errors within the 1% bound [16].

The origin of significant nonanalytic behavior lies in the dressings of hadrons by light pseudoscalar mesons. While many studies of chiral nonanalytic behavior are formulated in the infinite-volume continuum limit, it is important to understand that the nonanalytic behavior is intimately linked to the finite volume of the lattice. The momenta available to the hadrons participating in the loop integrals which give rise to the nonanalytic terms of the chiral expansion are modified in a finite volume. For P-wave intermediate states there is a threshold effect [9] where there is no strength in the momentum integral until the first nontrivial momentum $(2\pi/L)$ is reached. Even then the number of discrete momenta available to the integral is governed by the number of lattice sites (L/a).

Systematic errors in the extrapolation of the finite lattice spacing to the continuum limit have been minimized through the development of improved actions [17–19] displaying excellent scaling properties [20–22]. As such, understanding the entangled properties of chiral nonanalytic behavior on a finite volume at a quantitative level with systematic errors at the level of 1% is a problem which remains at the forefront of lattice gauge theory.

For the foreseeable future, extrapolations will continue to be required to connect lattice simulation results to physical observables. Hence, the development of systematically accurate chiral extrapolation techniques is of central importance to the field [13,14,23].

Fortunately it is possible to test the development of chiral extrapolation techniques today. The key point is that one can probe the chiral regime of quenched or partially quenched QCD using fermion actions with improved [18] or perfect [19] chiral symmetry properties. Thus, one can confront the analytic techniques of chiral effective field theory with numerical simulation results and test the extent to which effective field theory reproduces the exact results of numerical simulations.

This investigation will establish the leading chiral nonanalytic behavior of quark sector contributions to octet baryon magnetic moments in full, quenched and partially quenched QCD. As we will see, significant nonanalytic behavior remains for some quark-sector contributions to baryon magnetic moments making these observables ideal for the confrontation of effective field theory and lattice QCD.

Separation of the valence and sea-quark-loop contributions to the meson cloud of full QCD hadrons is a nontrivial task. Early calculations addressing the meson cloud of mesons employed a diagrammatic method [24]. The formal theory of quenched chiral perturbation theory (QχPT) was subsequently established in Ref. [25]. There, meson proper-

*Electronic address: dleinweb@physics.adelaide.edu.au; URL: http://www.physics.adelaide.edu.au/theory/staff/leinweber/

ties were examined in a graded-symmetry formulation where extra commuting ghost-quark fields are introduced to eliminate the dependence of the path integral on the fermion-matrix determinant. This approach was extended to the baryon sector in Ref. [26].

While the graded-symmetry formalism is essential to establishing the field theoretic properties of QχPT, it is desirable to formulate an efficient and perhaps more intuitive approach to the calculation of quenched chiral coefficients. Rather than introducing extra degrees of freedom to remove the effects of sea-quark loops, the approach described herein introduces a formalism for the identification and calculation of sea-quark-loop contributions to baryon properties, allowing the systematic separation of valence- and sea-quark contributions to baryon form factors in general. Upon removing the contributions of sea-quark-loops, one arrives at the conventional view of quenched chiral perturbation theory.

A brief account of these methods is published in Ref. [27]. Since this presentation, there has been a resurgence in quenched and partially quenched χPT calculations of baryon magnetic moments [28,29]. In particular, the magnetic moments of octet baryons have been examined [28] using the formal approach of QχPT [26]. There the leading-nonanalytic (LNA) behavior of the magnetic moment for each baryon of the octet is calculated. Upon summing the quark sector contributions obtained from the diagrammatic method presented here, one finds complete agreement between the diagrammatic and formal approaches. The approaches are equivalent.

In its standard implementation, the formal approach completely eliminates all sea-quark-loop contributions to quenched baryon moments. However, sea-quark loops do make a contribution to matrix elements in the quenched approximation. Insertion of the current in calculating the three-point correlation function provides pair(s) of quark-creation and annihilation operators. These can be contracted with the quark field operators of the hadron interpolating fields providing ''connected insertions'' of the current, or self-contracted to form a direct sea-quark-loop contribution or ''disconnected insertion'' of the current. The latter contributions to baryon electromagnetic form factors are under intense investigation in quenched simulations [30–33]. Hence in formulating quenched chiral perturbation theory it is important to provide an opportunity to include these particular sea-quark-loop contributions. A more flexible approach to the calculation of quenched chiral coefficients is desirable.

Moreover, the present calculations [28,29,34] of chiral nonanalytic behavior in baryon magnetic moments focus on bulk baryon properties. The formalism presented here provides a method for the isolation of individual quark sector contributions [35–40] to form factors in full, quenched and partially quenched QCD. Individual quark sector contributions to the nucleon magnetic moments are under experimental investigation [41–43] where the strange-quark contribution to the nucleon moment is of paramount interest. Understanding the manner in which quarks compose baryons is essential to a complete understanding of QCD.

In the process, we will see that it is possible to separate valence- and sea-quark contributions to baryon form factors in *full* QCD. This separation is of significant value as contributions from disconnected insertions of the current are difficult to determine in lattice QCD simulations. Moreover, chiral nonanalytic behavior of quark sector contributions can be significantly enhanced when direct sea-quark loop couplings to the current are removed.

In contrast to conventional calculations of chiral nonanalytic structure, $SU(3)$-flavor violations in both meson *and* baryon masses are accounted for in the following. These are particularly important for K-meson dressings of hyperons where the baryon mass splitting can be positive or negative, suppressing or enhancing contributions depending on whether the intermediate baryon is heavier or lighter respectively. Incorporation of the baryon mass splittings significantly alters the functional structure and associated curvature of the nonanalytic terms. $SU(3)$-flavor violations will also affect the analytic terms of the chiral expansion. The leading constant, the coefficient of m_π^2 ($\propto m_q$) etc. will all exhibit a strangeness dependence due to symmetry breaking. Ultimately, these coefficients will be determined by matching the chiral expansion to lattice QCD simulation results [13,14].

In principle, the axial couplings, D and F, are defined and specified in the chiral $SU(3)$-flavor symmetric limit. The mass dependence of the couplings is incorporated in the chiral expansion through higher-order terms. Upon formulating the chiral expansion in the $SU(2)$ limit with explicit and substantial $SU(3)$-flavor symmetry breaking as is physically realized, one can break the symmetry of the axial couplings. However, previous examinations of the chiral corrections to baryon axial currents suggest that such phenomenological flavor-symmetry breaking is small [44].

Similarly, $SU(3)$ flavor-symmetry breaking is often incorporated by allowing the decay constant of the kaon to exceed that of the pion, $f_K \simeq 1.2 f_\pi$. In the past, K-loop contributions were often found to be uncomfortably large when matching to phenomenology and the 30% reduction obtained in using f_K in place of f_π proved to be helpful [34]. However, it is not yet clear whether this phenomenological suppression of K-loops through the use of f_K is necessary when regulators suppressing short distance physics are used in chiral effective field theory.

To make the numerical results of this study readily accessible and of the widest utility, the established tree-level axial couplings $F=0.50$ and $D=0.76$ are adopted with the $SU(3)$-symmetric limit of $f_\pi = f_K = 93$ MeV for the meson decay constants.

In summary, the purpose of this study is as follows: (i) To provide the first calculation of the leading nonanalytic behavior of quark-flavor contributions to baryon magnetic moments in full QCD, (ii) quenched QCD, and (iii) partially quenched QCD. (iv) To separate valence- and sea-quark contributions to baryon form factors in *full* QCD at the individual quark-flavor level. (v) To extend previous baryon-moment calculations [28,29,34] to include both meson and baryon mass splittings in $SU(3)$-flavor violations, as is done for items (i) through (iv) above. (vi) To identify quark-flavor channels displaying significant chiral nonanalytic behavior in the quenched approximation or revealing the artifacts of the quenched approximation. (vii) To establish the diagrammatic

method for calculating the chiral coefficients of quenched and partially quenched QCD in the baryon sector. The method is rapid, intuitive and transparent, allowing complete flexibility in the consideration of quark contributions to baryon form factors.

It will become apparent that this technique and most of the results may be applied to other baryon form factor studies in general.

Section II presents the essential concepts for isolating and calculating sea-quark loop contributions to baryon properties and proves the technique via a consideration of baryon masses. The derivation of the quenched chiral coefficients for the quark-sector contributions to the quenched magnetic moments of octet baryons is described in Sec. III. The technique provides a separation of magnetic moment contributions into ''total'' full-QCD contributions, ''direct sea-quark loop'' and ''valence'' contributions of full-QCD. The latter are obtained by removing the direct-current coupling to sea-quark loops from the total contributions. Upon further removing ''indirect sea-quark loop'' contributions, one obtains the ''quenched valence'' contributions, the conventional view of the quenched approximation. We will use the quoted terms for reference to these contributions in the following. Section III also accounts for both baryon mass and meson mass violations of $SU(3)$-flavor symmetry. The quenched η' gives rise to new nonanalytic behavior [28] and this is briefly reviewed in Sec. III D.

A comprehensive examination of the individual quark-sector contributions to octet baryon magnetic moments is presented in Sec. IV. General expressions are accompanied by numerical evaluations to identify channels of particular interest. Partially quenched results are presented in Sec. V. Section VI provides a summary of the highlights of the findings.

II. QUENCHED BARYON MASSES

A. Formalism

The $SU(3)$-flavor invariant couplings are described in the standard notation by defining

$$B=\begin{pmatrix} \frac{\Sigma^0}{\sqrt{2}}+\frac{\Lambda}{\sqrt{6}} & \Sigma^+ & p \\ \Sigma^- & -\frac{\Sigma^0}{\sqrt{2}}+\frac{\Lambda}{\sqrt{6}} & n \\ \Xi^- & \Xi^0 & -\frac{2\Lambda}{\sqrt{6}} \end{pmatrix}, \tag{1}$$

$$P_{\rm oct}=\begin{pmatrix} \frac{\pi^0}{\sqrt{2}}+\frac{\eta}{\sqrt{6}} & \pi^+ & K^+ \\ \pi^- & -\frac{\pi^0}{\sqrt{2}}+\frac{\eta}{\sqrt{6}} & K^0 \\ K^- & \overline{K^0} & -\frac{2\eta}{\sqrt{6}} \end{pmatrix}, \tag{2}$$

and

$$P_{\rm sin}=\frac{1}{\sqrt{3}}\,{\rm diag}(\eta',\eta',\eta'). \tag{3}$$

The $SU(3)$-invariant combinations are

$$[\bar{B}BP]_F={\rm Tr}(\bar{B}P_{\rm oct}B)-{\rm Tr}(\bar{B}BP_{\rm oct}), \tag{4}$$

$$[\bar{B}BP]_D={\rm Tr}(\bar{B}P_{\rm oct}B)+{\rm Tr}(\bar{B}BP_{\rm oct}), \tag{5}$$

$$[\bar{B}BP]_S={\rm Tr}(\bar{B}B){\rm Tr}(P_{\rm sin}). \tag{6}$$

The following calculations are simplified through the use of the corresponding interaction Lagrangians [45]. The octet interaction Lagrangian is

$$\begin{aligned}\mathcal{L}_{\rm int}^{\rm oct}=&-f_{NN\pi}(\bar{N}\tau^{\rm T}N)\cdot\pi+if_{\Sigma\Sigma\pi}(\bar{\Sigma}\times\Sigma)\cdot\pi\\&-f_{\Lambda\Sigma\pi}(\bar{\Lambda}\Sigma+\bar{\Sigma}\Lambda)\cdot\pi-f_{\Xi\Xi\pi}(\bar{\Xi}\tau^{\rm T}\Xi)\cdot\pi\\&-f_{\Lambda NK}[(\bar{N}K)\Lambda+\bar{\Lambda}(\bar{K}N)]\\&-f_{\Xi\Lambda K}[(\bar{\Xi}K_c)\Lambda+\bar{\Lambda}(\bar{K_c}\Xi)]\\&-f_{\Sigma NK}[\bar{\Sigma}\cdot(\bar{K}\tau^{\rm T}N)+(\bar{N}\tau^{\rm T}K)\cdot\Sigma]\\&-f_{\Xi\Sigma K}[\bar{\Sigma}\cdot(\bar{K_c}\tau^{\rm T}\Xi)+(\bar{\Xi}\tau^{\rm T}K_c)\cdot\Sigma]-f_{NN\eta}(\bar{N}N)\,\eta\\&-f_{\Lambda\Lambda\eta}(\bar{\Lambda}\Lambda)\,\eta-f_{\Sigma\Sigma\eta}(\bar{\Sigma}\cdot\Sigma)\,\eta-f_{\Xi\Xi\eta}(\bar{\Xi}\Xi)\,\eta\end{aligned} \tag{7}$$

and the singlet interaction Lagrangian is

$$\begin{aligned}\mathcal{L}_{\rm int}^{\rm sin}=&-f_{NN\eta'}(\bar{N}N)\,\eta'-f_{\Lambda\Lambda\eta'}(\bar{\Lambda}\Lambda)\,\eta'-f_{\Sigma\Sigma\eta'}(\bar{\Sigma}\cdot\Sigma)\,\eta'\\&-f_{\Xi\Xi\eta'}(\bar{\Xi}\Xi)\,\eta',\end{aligned} \tag{8}$$

where

$$N=\begin{pmatrix}p\\n\end{pmatrix},\quad \Xi=\begin{pmatrix}\Xi^0\\\Xi^-\end{pmatrix},$$

$$K=\begin{pmatrix}K^+\\K^0\end{pmatrix},\quad K_c=\begin{pmatrix}\overline{K^0}\\-K^-\end{pmatrix}. \tag{9}$$

The octet meson-baryon couplings are expressed in terms of the F and D coupling coefficients as follows:

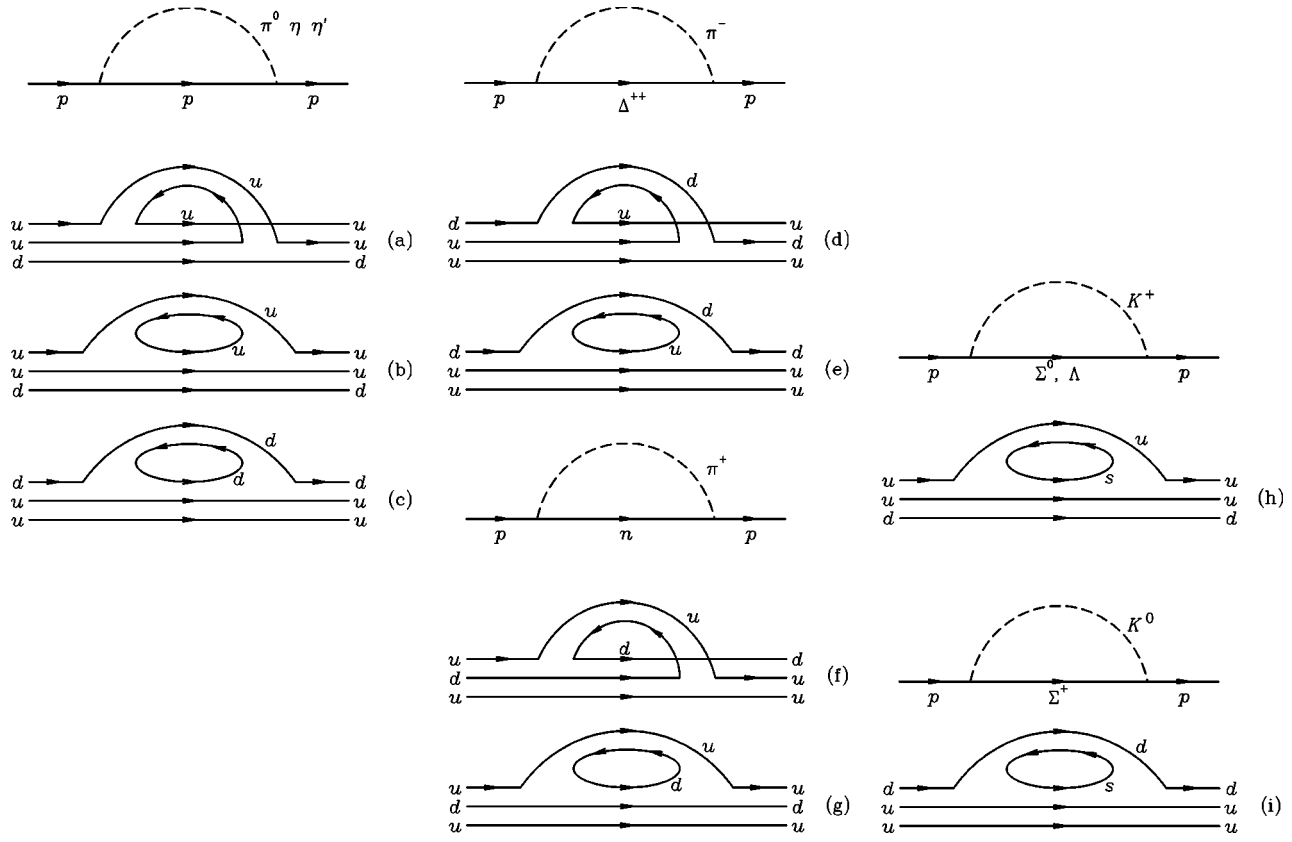

FIG. 1. The pseudo-Goldstone meson cloud of the proton and associated quark flow diagrams.

$$f_{NN\pi}=F+D, \qquad f_{\Lambda NK}=-\frac{1}{\sqrt{3}}(3F+D),$$

$$f_{NN\eta}=\frac{1}{\sqrt{3}}(3F-D), \quad f_{\Sigma\Sigma\pi}=2F,$$

$$f_{\Xi\Lambda K}=\frac{1}{\sqrt{3}}(3F-D), \quad f_{\Lambda\Lambda\eta}=-\frac{2}{\sqrt{3}}D,$$

$$f_{\Lambda\Sigma\pi}=\frac{2}{\sqrt{3}}D, \qquad f_{\Sigma NK}=D-F,$$

$$f_{\Sigma\Sigma\eta}=\frac{2}{\sqrt{3}}D, \qquad f_{\Xi\Xi\pi}=F-D,$$

$$f_{\Xi\Sigma K}=-(F+D), \qquad f_{\Xi\Xi\eta}=-\frac{1}{\sqrt{3}}(3F+D), \quad (10)$$

and the singlet couplings satisfy

$$f_{NN\eta'}=f_{\Lambda\Lambda\eta'}=f_{\Sigma\Sigma\eta'}=f_{\Xi\Xi\eta'}. \quad (11)$$

The light quark content of

$$|\eta'\rangle=\frac{1}{\sqrt{3}}(|\overline{uu}\rangle+|\overline{dd}\rangle+|\overline{ss}\rangle), \quad (12)$$

and

$$|\eta\rangle=\frac{1}{\sqrt{6}}(|\overline{uu}\rangle+|\overline{dd}\rangle-2|\overline{ss}\rangle), \quad (13)$$

mesons suggests

$$f_{NN\eta'}=\sqrt{2}f_{NN\eta}. \quad (14)$$

This relation between nucleon octet and singlet couplings is commonly used in QχPT calculations to estimate η' couplings to octet baryons. In the following, numerical estimates are based on the tree-level axial couplings $F=0.50$ and $D=0.76$ with $f_\pi=f_K=93$ MeV.

The leading-nonanalytic term of the chiral expansion provides the dominant source of rapid variation in baryon magnetic moments. Taking the N-Δ mass splitting to be of zeroth chiral order, the Δ resonance provides the next-to-leading nonanalytic (NLNA) contribution. This contribution makes only a small correction to the proton magnetic moment obtained from the chiral extrapolation of lattice QCD simulation results. The N-Δ mass splitting suppresses the nonanalytic curvature, and when combined with the analytic terms of the chiral expansion, only a small enhancement of the proton moment is observed. As the NLNA Δ contribution is added, the proton moment increases from 2.61 to 2.66 μ_N [15]. This 2% effect at the physical point is unlikely to be observed in lattice QCD simulation results for some time. As such, we do not encumber the reader with these small contributions.

TABLE I. Meson-cloud contributions of Fig. 1 in full QCD. η and η' masses are set degenerate with the pion in anticipation of quenching the theory.

Fig.	Channel	Mass	Coupling	Coupling
a,b,c	$p\pi^0$	$N\pi$	$f^2_{NN\pi}$	$(F+D)^2$
a,b,c	$p\eta$	$N\pi$	$f^2_{NN\eta}$	$(3F-D)^2/3$
a,b,c	$p\eta'$	$N\pi$	$f^2_{NN\eta'}$	$2(3F-D)^2/3$
f,g	$n\pi^+$	$N\pi$	$2f^2_{NN\pi}$	$2(F+D)^2$
h	ΛK^+	ΛK	$f^2_{\Lambda NK}$	$(3F+D)^2/3$
h	$\Sigma^0 K^+$	ΣK	$f^2_{\Sigma NK}$	$(D-F)^2$
i	$\Sigma^+ K^0$	ΣK	$2f^2_{\Sigma NK}$	$2(D-F)^2$

TABLE II. Sea-quark-loop contributions of Fig. 1.

Fig.	Channel	Mass	Coupling	Coupling
b	ΛK^+	$N\pi$	$f^2_{\Lambda NK}$	$(3F+D)^2/3$
b	$\Sigma^0 K^+$	$N\pi$	$f^2_{\Sigma NK}$	$(D-F)^2$
c	$\Sigma^+ K^0$	$N\pi$	$2f^2_{\Sigma NK}$	$2(D-F)^2$
e	$\Sigma^+ K^0$	$N\pi$	$2f^2_{\Sigma NK}$	$2(D-F)^2$
g	ΛK^+	$N\pi$	$f^2_{\Lambda NK}$	$(3F+D)^2/3$
g	$\Sigma^0 K^+$	$N\pi$	$f^2_{\Sigma NK}$	$(D-F)^2$
h	ΛK^+	ΛK	$f^2_{\Lambda NK}$	$(3F+D)^2/3$
h	$\Sigma^0 K^+$	ΣK	$f^2_{\Sigma NK}$	$(D-F)^2$
i	$\Sigma^+ K^0$	ΣK	$2f^2_{\Sigma NK}$	$2(D-F)^2$

B. Baryon mass

To calculate the quenched chiral coefficients, we begin by calculating the total full-QCD contribution in the limit where the η and η' mesons are taken to be degenerate with the pion. In the quenched approximation, quark loops which otherwise break this degeneracy are absent. The quark flow diagrams of Fig. 1 illustrate the processes which give rise to the LNA behavior of proton observables. Table I summarizes the contributions of the π-, η-, η'- and K-cloud diagrams of Fig. 1 labeled by the corresponding quark-flow diagrams. Summation of these couplings and incorporation of the factors from the loop integral provides the LNA term proportional to m_π^3 of

$$-(3F^2+D^2)\frac{m_\pi^3}{8\pi f_\pi^2}. \tag{15}$$

The separation of the meson cloud into valence and sea-quark contributions is shown in the quark-flow diagrams labeled by letters. To quench the theory, one must understand the chiral behavior of the valence-quark loops of Figs. 1(a), (d) and (f) and the sea-quark loops of Figs. 1(b), (c), (e), (g), (h) and (i) separately. If one can isolate the behavior of the diagrams involving a quark loop, then one can use the known LNA behavior of the full meson-based diagrams to extract the corresponding valence-loop contributions.

For example, Fig. 1(b) involves a u-quark loop where no exchange term is possible. Thus the u-quark in the loop is distinguishable from all the other quarks in the diagram. The chiral structure of this diagram is therefore identical to that for a ''strange'' quark loop, as illustrated in Fig. 1(h) ($p\to K^+\Sigma^0$ or $p\to K^+\Lambda$) provided the ''strange'' quark in *this* case is understood to have the same mass as the u-quark.

Similarly, the corresponding hadron diagram which gives rise to the LNA structure of Fig. 1(c) is therefore the K^0-loop diagram of Fig. 1(i), with the distinguishable ''strange'' quark mass set equal to the mass of the d-quark. That is, the intermediate Σ-baryon mass appearing in the K^0-loop diagram is degenerate with the nucleon. Similarly, the ''kaon'' mass is degenerate with the pion.

The sum of the first two lines of Table II provides the contribution of diagram Fig. 1(b). The third line provides the contribution of Fig. 1(c). Similar arguments allow one to establish the remaining loop contributions to the light-meson cloud. Summing the couplings of Table II indicates sea-quark-loops contribute a term

$$-(9F^2-6FD+5D^2)\frac{m_\pi^3}{24\pi f_\pi^2}, \tag{16}$$

to the LNA behavior of the nucleon such that the net quenched contribution proportional to m_π^3 is

$$-(3FD-D^2)\frac{m_\pi^3}{12\pi f_\pi^2}, \tag{17}$$

in agreement with the formal approach of Labrenz and Sharpe [26]. We note that the kaon-cloud contributions of Fig. 1(h) and (i) are pure sea contributions and trivially vanish in subtracting sea-contributions from total contributions as outlined above.

III. BARYON MAGNETIC MOMENTS

A. Quark-sector contributions to the proton

The LNA contribution to baryon magnetic moments proportional to m_π or m_K has its origin in couplings of the electromagnetic (EM) current to the meson propagating in the intermediate meson-baryon state. In order to pick out a

TABLE III. Determination of the total u-quark contribution to the proton magnetic moment as illustrated in Fig. 1.

Diagram	Channel	Mass	Charge	Term	β	χ
f,g	$n\pi^+$	$N\pi$	$+1$	$+2f^2_{NN\pi}m_\pi$	$-(F+D)^2$	-6.87
h	$\Sigma^0 K^+$	ΣK	$+1$	$+f^2_{\Sigma NK}m_{N\Sigma K}$	$-(D-F)^2/2$	-0.15
h	ΛK^+	ΛK	$+1$	$+f^2_{\Lambda NK}m_{N\Lambda K}$	$-(3F+D)^2/6$	-3.68

TABLE IV. Determination of direct *u*-quark sea-quark loop contributions to the proton magnetic moment as illustrated in Fig. 1.

Diagram	Channel	Mass	Charge	Term	β	χ
b	ΛK^+	$N\pi$	-1	$-f^2_{\Lambda NK} m_\pi$	$(3F+D)^2/6$	$+3.68$
b	$\Sigma^0 K^+$	$N\pi$	-1	$-f^2_{\Sigma NK} m_\pi$	$(D-F)^2/2$	$+0.15$
e	$\Sigma^+ K^0$	$N\pi$	-1	$-2f^2_{\Sigma NK} m_\pi$	$(D-F)^2$	$+0.29$
Total						$+4.12$

particular quark-flavor contribution, one sets the electric charge for the quark of interest to one and the charge of all other flavors to zero.

Tables III through V report results for the *u*-quark in the proton. The total contributions are calculated in the standard way, but with charge assignments for the intermediate mesons (indicated in the ''charge'' column) reflecting in this case $q_u=1$ and $q_d=q_s=0$. The extra baryon subscripts on the meson masses are a reminder of the baryons participating in the diagram to facilitate more accurate treatments of the loop integral in which baryon mass splittings are taken into account. The LNA contribution is

$$\beta \frac{m_N}{8\pi f_\pi^2} m_\pi \equiv \chi m_\pi \tag{18}$$

with β and χ indicated in the last two columns. Throughout the following, the units of χ are μ_N/GeV, such that when multiplied by the pion mass in GeV, one obtains magnetic moment contributions in units of the nuclear magneton, μ_N.

The ''direct sea-quark-loop contributions'' indicated in Table IV are contributions in which the EM current couples to a sea-quark loop, in this case a *u* quark. Using the techniques described in Sec. II, one can calculate the contributions of these loops alone to the baryon magnetic moment. The ''mass'' column of Table IV is a reminder that the mass of the ''kaon'' considered in determining the coupling is actually the pion mass for Figs. 1(b) and (e). These diagrams will contribute, even in the quenched approximation, when disconnected insertions of the EM current are included in simulations [30–33].

Subtraction of these sea-quark-loop contributions from the total contributions of Table III leaves a net valence contribution of $-11.0m_\pi - 0.15m_{N\Sigma K} - 3.68m_{N\Lambda K}$ in *full* QCD.

Table V focuses on diagrams in which the EM current couples to a valence quark in a meson composed with a sea-quark loop. These are the ''indirect sea-quark loop'' contributions. Subtracting off these couplings from the valence contribution provides the net quenched valence contribution of $-3.33m_\pi$.

Tables VI through VIII provide a similar analysis of the *d* quark in the proton, where $q_d=1$ and $q_u=q_d=0$. Subtraction of the direct sea-quark loop contributions of Table VII from the total contributions of Table VI leaves a net valence contribution of $2.75m_\pi - 0.29m_{N\Sigma K}$. Further removal of the indirect sea-quark loops of Table VIII provides the final net *d*-quark quenched valence contribution to the proton moment of $+3.33m_\pi$.

Table IX describes the *s*-quark contributions to the proton magnetic moment, where $q_s=1$ and $q_u=q_d=0$. As there are no *s* valence quarks in the proton, the contributions are purely sea-quark-loop contributions. The net valence contribution is zero and there are no further quenching considerations.

Charge symmetry provides the quark-sector contributions to the neutron magnetic moment. For unit charge quarks, $d_n=u_p$, $u_n=d_p$ and $s_n=s_p$.

The QCD Lagrangian is flavor blind in the $SU(3)$-flavor symmetry limit. This independence from quark flavor is manifest in Tables IV, VII and IX for the direct sea-quark loop contributions to the proton form factor. In each case there are three channels for the coupling, β. Indeed the *u* and *d* direct sea-quark loop contributions are exactly equal. However $SU(3)$-flavor symmetry breaking due to the massive *s* quark requires one to track the masses of intermediate mesons and baryons, and this introduces the K, Σ and Λ masses in Table IX.

$SU(3)$-flavor symmetry is also manifest in the indirect sea-quark loop contributions to the proton magnetic moment. For example, the *u*-quark indirect sea-quark loop result receives contributions from each of *u*, *d* and *s* quark loops in Figs. 1(b), 1(g) and 1(h). Each of these contributions appear-

TABLE V. Indirect sea-quark loop contributions from *u* valence quarks to the proton magnetic moment. Here, the *u*-valence quark forms a meson composed with a sea-quark loop as illustrated in Fig. 1.

Diagram	Channel	Mass	Charge	Term	β	χ
b	ΛK^+	$N\pi$	$+1$	$+f^2_{\Lambda NK} m_\pi$	$-(3F+D)^2/6$	-3.68
b	$\Sigma^0 K^+$	$N\pi$	$+1$	$+f^2_{\Sigma NK} m_\pi$	$-(D-F)^2/2$	-0.15
g	ΛK^+	$N\pi$	$+1$	$+f^2_{\Lambda NK} m_\pi$	$-(3F+D)^2/6$	-3.68
g	$\Sigma^0 K^+$	$N\pi$	$+1$	$+f^2_{\Sigma NK} m_\pi$	$-(D-F)^2/2$	-0.15
h	$\Sigma^0 K^+$	ΣK	$+1$	$+f^2_{\Sigma NK} m_{N\Sigma K}$	$-(D-F)^2/2$	-0.15
h	ΛK^+	ΛK	$+1$	$+f^2_{\Lambda NK} m_{N\Lambda K}$	$-(3F+D)^2/6$	-3.68

TABLE VI. Determination of the total *d*-quark contribution to the proton magnetic moment as illustrated in Fig. 1.

Diagram	Channel	Mass	Charge	Term	β	χ
f,g	$n\pi^+$	$N\pi$	-1	$-2f^2_{NN\pi}m_\pi$	$(F+D)^2$	$+6.87$
i	Σ^+K^0	ΣK	$+1$	$+2f^2_{\Sigma NK}m_{N\Sigma K}$	$-(D-F)^2$	-0.29

TABLE VII. Determination of direct *d*-quark sea-quark loop contributions to the proton magnetic moment as illustrated in Fig. 1.

Diagram	Channel	Mass	Charge	Term	β	χ
c	Σ^+K^0	$N\pi$	-1	$-2f^2_{\Sigma NK}m_\pi$	$(D-F)^2$	$+0.29$
g	ΛK^+	$N\pi$	-1	$-f^2_{\Lambda NK}m_\pi$	$(3F+D)^2/6$	$+3.68$
g	Σ^0K^+	$N\pi$	-1	$-f^2_{\Sigma NK}m_\pi$	$(D-F)^2/2$	$+0.15$
Total						$+4.12$

TABLE VIII. Indirect sea-quark loop contributions from *d* valence quarks to the proton magnetic moment. Here the *d*-valence quark forms a meson composed with a sea-quark loop as illustrated in Fig. 1.

Diagram	Channel	Mass	Charge	Term	β	χ
c	Σ^+K^0	$N\pi$	$+1$	$2f^2_{\Sigma NK}m_\pi$	$-(D-F)^2$	-0.29
e	Σ^+K^0	$N\pi$	$+1$	$2f^2_{\Sigma NK}m_\pi$	$-(D-F)^2$	-0.29
i	Σ^+K^0	ΣK	$+1$	$+2f^2_{\Sigma NK}m_{N\Sigma K}$	$-(D-F)^2$	-0.29

TABLE IX. Determination of the total *s*-quark contribution to the proton magnetic moment as illustrated in Fig. 1. As there are no *s* valence quarks in the proton, the contributions are purely sea-quark-loop contributions.

Diagram	Channel	Mass	Charge	Term	β	χ
h	Σ^0K^+	ΣK	-1	$-f^2_{\Sigma NK}m_{N\Sigma K}$	$(D-F)^2/2$	0.15
h	ΛK^+	ΛK	-1	$-f^2_{\Lambda NK}m_{N\Lambda K}$	$(3F+D)^2/6$	3.68
i	Σ^+K^0	ΣK	-1	$-2f^2_{\Sigma NK}m_{N\Sigma K}$	$(D-F)^2$	0.29

TABLE X. Determination of the total *u*-quark contribution to the Σ^+ magnetic moment as illustrated in Fig. 2.

Diagram	Channel	Mass	Charge	Term	β	χ
c	$\Sigma^0\pi^+$	$\Sigma\pi$	$+1$	$f^2_{\Sigma\Sigma\pi}m_{\Sigma\Sigma\pi}$	$-2F^2$	-2.16
c	$\Lambda\pi^+$	$\Lambda\pi$	$+1$	$f^2_{\Sigma\Lambda\pi}m_{\Sigma\Lambda\pi}$	$-2D^2/3$	-1.67
g,h	Ξ^0K^+	ΞK	$+1$	$2f^2_{\Sigma\Xi K}m_{\Sigma\Xi K}$	$-(F+D)^2$	-6.87

TABLE XI. Determination of direct *u*-quark sea-quark loop contributions to the Σ^+ magnetic moment as illustrated in Fig. 2.

Diagram	Channel	Mass	Charge	Term	β	χ
b	$\Sigma^0\pi^+$	$\Sigma\pi$	-1	$-f^2_{\Sigma\Sigma\pi}m_{\Sigma\Sigma\pi}$	$2F^2$	$+2.16$
b	$\Lambda\pi^+$	$\Lambda\pi$	-1	$-f^2_{\Sigma\Lambda\pi}m_{\Sigma\Lambda\pi}$	$2D^2/3$	$+1.67$
e	$p\overline{K^0}$	NK	-1	$-2f^2_{\Sigma NK}m_{\Sigma NK}$	$(D-F)^2$	$+0.29$

ing in Table V is equal up to symmetry breaking in the meson and baryon masses. Similar results hold for the *d*-valence quark of the proton in Table VIII.

The flavor-blind nature of QCD makes it trivial to extend this calculation of quenched quark-sector magnetic moments to the partially quenched theory. As new flavors are introduced through the use of dynamically generated gauge fields, one simply adds the direct and indirect sea-quark loop contributions evaluated here to the quenched results, keeping track of the meson mass of the valence-sea meson. The latter is simple to do as we have already isolated each valence quark flavor contribution to the baryon moment. This is described in further detail in Sec. V.

B. Quark-sector contributions to Σ^+

Tables X through XII describe the various LNA contributions of the *u* quark to the Σ^+ magnetic moment derived from Fig. 2. The total contribution of the *u* quark alone is isolated by setting the charge of the *s* and *d* quarks to zero, and otherwise using standard techniques. The LNA behavior of the *u*-quark contribution to the Σ^+ magnetic moment is $-2.16m_{\Sigma\Sigma\pi}-1.67m_{\Sigma\Lambda\pi}-6.87m_{\Sigma\Xi K}$. Sea-quark-loop contributions are isolated by using meson-baryon couplings where quark loops of *u* and *s* quark flavors (the valence flavors of Σ^+) are replaced by a *d* quark. Table XI summarizes the direct sea-quark loop contributions. Subtracting these contributions leaves a net valence contribution of $-0.29m_{\Sigma NK}-4.32m_{\Sigma\Sigma\pi}-3.33m_{\Sigma\Lambda\pi}-6.87m_{\Sigma\Xi K}$ in full QCD. Table XII describes indirect sea-quark loop contributions from *u* valence quarks in mesons formed with a sea-quark loop. Removing these contributions provides the net quenched *u*-valence contribution of $-0.29m_{\Sigma NK}-0.29m_{\Sigma NK}-3.04m_{\Sigma\Xi K}$.

The *d*-quark contributions to the LNA behavior of the Σ^+ magnetic moment are pure sea in origin. Therefore the total contributions are the sea contributions such that the valence *d*-quark contributions vanish. Table XIII summarizes the contributions.

s-quark contributions to the Σ^+ magnetic moment are summarized in Tables XIV through XVI. Removal of the direct sea-quark-loop contributions from the total contributions provides an *s*-valence contribution of $-0.29m_{\Sigma NK}+3.04m_{\Sigma\Xi K}-0.29m_{\Sigma\Sigma\eta_s}$ in full QCD. Further removal of the indirect sea-quark loop contributions of Table XVI provides the net quenched *s*-valence contribution of $+0.29m_{\Sigma NK}+3.04m_{\Sigma\Xi K}$.

Charge symmetry provides the quark sector contributions to the Σ^- baryon, while the Σ^0-baryon results are obtained from the isospin average of Σ^+ and Σ^-.

The $SU(3)$-flavor symmetry of the direct sea-quark-loop contributions to the Σ^+ baryon magnetic moment is manifest throughout Tables XI, XIII and XV. However, the implementation of $SU(3)$-flavor breaking via the hadron masses hides the flavor symmetry in the results summarized in Sec. IV, where both meson and baryon mass splittings are maintained. $SU(3)$-flavor breaking gives rise to very different behaviors for these contributions. This is particularly true in the common application of holding the strange-quark mass fixed while varying the light *u* and *d* masses. In this case the η_s meson mass is constant.

C. Λ and Ξ baryons

The derivation of the quark sector contributions to Ξ baryons proceeds in precisely the same manner as that for the Σ baryons. As there are no new concepts, derivation is left as an exercise for the interested reader. Ξ-baryon results are summarized in Sec. IV.

However, the flavor singlet structure of the Λ baryon presents a problem to the approach described thus far. The necessary presence of *u*-, *d*- and *s*-quark flavors simultaneously, appears to require the introduction of a fourth quark flavor and its associated $SU(4)$ couplings to describe the discon-

TABLE XII. Indirect sea-quark loop contributions from *u* valence quarks to the Σ^+ magnetic moment. Here the *u*-valence quark forms a meson composed with a sea-quark loop as illustrated in Fig. 2.

Diagram	Channel	Mass	Charge	Term	β	χ
b	$\Sigma^0\pi^+$	$\Sigma\pi$	$+1$	$f^2_{\Sigma\Sigma\pi}m_{\Sigma\Sigma\pi}$	$-2F^2$	-2.16
b	$\Lambda\pi^+$	$\Lambda\pi$	$+1$	$f^2_{\Sigma\Lambda\pi}m_{\Sigma\Lambda\pi}$	$-2D^2/3$	-1.67
c	$\Sigma^0\pi^+$	$\Sigma\pi$	$+1$	$f^2_{\Sigma\Sigma\pi}m_{\Sigma\Sigma\pi}$	$-2F^2$	-2.16
c	$\Lambda\pi^+$	$\Lambda\pi$	$+1$	$f^2_{\Sigma\Lambda\pi}m_{\Sigma\Lambda\pi}$	$-2D^2/3$	-1.67
h	$\Sigma^0\pi^+$	ΞK	$+1$	$f^2_{\Sigma\Sigma\pi}m_{\Sigma\Xi K}$	$-2F^2$	-2.16
h	$\Lambda\pi^+$	ΞK	$+1$	$f^2_{\Sigma\Lambda\pi}m_{\Sigma\Xi K}$	$-2D^2/3$	-1.67

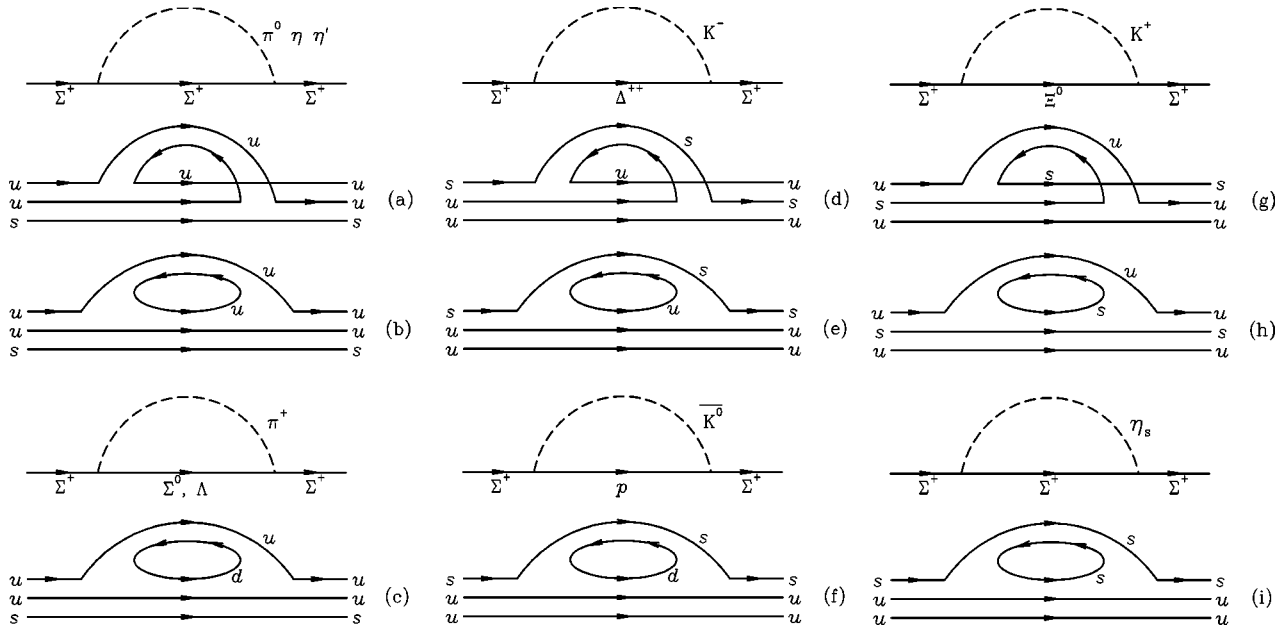

FIG. 2. The pseudo-Goldstone meson cloud of Σ^+ and associated quark flow diagrams.

nected sea-quark loop contributions.

Fortunately one can exploit the $SU(3)$-flavor symmetry relation among octet baryons. Such a relation is manifest in two- and three-point correlation functions for the Λ [35]. Denoting the two-point correlation function for Σ^0 as $\Sigma^0_s(x)$, one has

$$\Lambda(x)=\frac{1}{3}[2\Sigma^0_u(x)+2\Sigma^0_d(x)-\Sigma^0_s(x)], \tag{19}$$

where $\Sigma^0_s(x)$ has symmetry between u and d quarks, $\Sigma^0_u(x)$ has symmetry between s and d quarks, and similarly $\Sigma^0_d(x)$ has symmetry between u and s quarks. Just as

$$\Sigma^0_s(x)=\frac{1}{2}[\Sigma^+(x)+\Sigma^-(x)], \tag{20}$$

one also has

$$\Sigma^0_u(x)=\frac{1}{2}[n(x)+\Xi^0(x)], \tag{21}$$

and

$$\Sigma^0_d(x)=\frac{1}{2}[p(x)+\Xi^-(x)], \tag{22}$$

in the $SU(3)$-flavor limit, such that

$$\Lambda(x)=\frac{1}{3}\Big(p(x)+n(x)+\Xi^0(x)+\Xi^-(x) - \frac{1}{2}[\Sigma^+(x)+\Sigma^-(x)]\Big). \tag{23}$$

Note that this relation holds for any electric-charge assignments to the quark flavors, such that individual quark-flavor contributions can be resolved.

Of course it is essential to recover $SU(3)$-flavor violations. To do this one begins exactly as for the proton or Σ^+ described above by constructing the quark-flow diagrams describing the one-loop meson cloud of the Λ. The couplings of all sea-quark loop contributions can be related to the three quark-flow diagrams of Fig. 3. Unknown couplings f^2_u, f^2_d and f^2_s are introduced to describe the couplings of diagrams (a), (b) and (c) respectively. Our working approximation of exact $SU(2)$-isospin symmetry at the current-quark level provides $f^2_d=f^2_u$ in Λ, leaving two parameters, f^2_u and f^2_s, to be determined via the $SU(3)$ relation of Eq. (23). As both the light- and strange-quark contributions to the Λ moment

TABLE XIII. Determination of the total d-quark contribution to the Σ^+ magnetic moment as illustrated in Fig. 2. d-quark contributions are purely sea in origin such that the valence contribution vanishes.

Diagram	Channel	Mass	Charge	Term	β	χ
c	$\Sigma^0\pi^+$	$\Sigma\pi$	-1	$-f^2_{\Sigma\Sigma\pi}m_{\Sigma\Sigma\pi}$	$2F^2$	$+2.16$
c	$\Lambda\pi^+$	$\Lambda\pi$	-1	$-f^2_{\Sigma\Lambda\pi}m_{\Sigma\Lambda\pi}$	$2D^2/3$	$+1.67$
f	$p\overline{K^0}$	NK	-1	$-2f^2_{\Sigma NK}m_{\Sigma NK}$	$(D-F)^2$	$+0.29$

TABLE XIV. Determination of the total *s*-quark contribution to the Σ^+ magnetic moment as illustrated in Fig. 2.

Diagram	Channel	Mass	Charge	Term	β	χ
f	$p\overline{K^0}$	NK	$+1$	$2f^2_{\Sigma NK}m_{\Sigma NK}$	$-(D-F)^2$	-0.29
g,h	Ξ^0K^+	ΞK	-1	$-2f^2_{\Sigma\Xi K}m_{\Sigma\Xi K}$	$(F+D)^2$	$+6.87$

can be resolved, there are two $SU(3)$ relations to constrain the two parameters f_u^2 and f_s^2. This is particularly easy, when one recalls that the indirect sea-quark loop contribution from a u or s valence quark participating in a meson constructed with a sea-quark loop is proportional to either f_u^2 or f_s^2 alone. Results are summarized in Sec. IV.

D. Quenched exotics

The double hair-pin graph of Fig. 4 associated with the quenched-η' meson gives rise to new singular $\log(m_\pi)$ behavior in the chiral limit [28]. This logarithmic term provides a correction to the tree-level term. The contribution has its origin in the loop integral of Fig. 4(a) corresponding to

$$-i\frac{16\pi^2}{3}\int\frac{d^4q}{(2\pi)^4}\frac{q^2-(v\cdot q)^2}{[v\cdot q+i\epsilon]^2[q^2-m_1^2+i\epsilon][q^2-m_2^2+i\epsilon]}. \tag{24}$$

For equal singlet-meson masses $m_1=m_2$, as in the quark flow of Fig. 4(b), this integral provides the nonanalytic behavior of

$$\log\left(\frac{m^2}{\Lambda^2}\right). \tag{25}$$

However, Fig. 4(c) indicates that the meson masses in the double hair-pin graph need not be equal when considering hyperon magnetic moments. Here the η'-meson masses m_1 and m_2 may correspond to different quark-antiquark sources; e.g. $\eta'(u\overline{u})$ versus $\eta'(s\overline{s})$. When $m_1\neq m_2$, one finds a nonanalytic contribution of

$$\frac{m_1^2\log\left(\frac{m_1^2}{\Lambda^2}\right)-m_2^2\log\left(\frac{m_2^2}{\Lambda^2}\right)}{m_1^2-m_2^2}. \tag{26}$$

Hence, for the hyperons, one must isolate the doubly and singly represented quark sector couplings to η' mesons.

Consider for example, η' couplings for Σ^+ involving u quarks. The transition $\Sigma^+\to\Sigma^+\pi^0$ involves u quarks alone at one loop and can be used to determine the η'_u coupling. The Σ^+-π^0 coupling is $f_{\Sigma\Sigma\pi}=2F$. Since

$$|\pi^0\rangle=\frac{1}{\sqrt{2}}(|u\overline{u}\rangle-|d\overline{d}\rangle),$$

$$|\eta\rangle=\frac{1}{\sqrt{6}}(|u\overline{u}\rangle+|d\overline{d}\rangle-2|s\overline{s}\rangle),$$

$$|\eta'\rangle=\frac{1}{\sqrt{3}}(|u\overline{u}\rangle+|d\overline{d}\rangle+|s\overline{s}\rangle),$$

one has

$$|u\overline{u}\rangle=\frac{1}{\sqrt{6}}(\sqrt{3}|\pi^0\rangle+|\eta\rangle+\sqrt{2}|\eta'\rangle). \tag{27}$$

The η'_u coupling is $\sqrt{2/3}$ of the pion coupling to $|u\overline{u}\rangle$; i.e. $2\sqrt{2/3}F$.

For the singly represented quark sector, consider $\Xi^0\to\Xi^0\pi^0$ involving u-quarks alone at one loop. Here the u-quark coupling is $f_{\Xi\Xi\pi}=(F-D)$, such that the η'_u coupling to Ξ baryons is $\sqrt{2/3}(F-D)$.

To check this separation of quark sector contributions to η' contributions, consider the proton. Here the contribution to intermediate η' states is

$$\frac{2}{3}\{4F^2I(\eta_u,\eta_u)+2\cdot 2F(F-D)I(\eta_u,\eta_d)+(F-D)^2I(\eta_d,\eta_d)\}, \tag{28}$$

TABLE XV. Determination of direct *s*-quark sea-quark loop contributions to the Σ^+ magnetic moment as illustrated in Fig. 2. η_s denotes the $s\overline{s}$ η meson.

Diagram	Channel	Mass	Charge	Term	β	χ
h	$\Sigma^0\pi^+$	ΞK	-1	$-f^2_{\Sigma\Sigma\pi}m_{\Sigma\Xi K}$	$2F^2$	$+2.16$
h	$\Lambda\pi^+$	ΞK	-1	$-f^2_{\Sigma\Lambda\pi}m_{\Sigma\Xi K}$	$2D^2/3$	$+1.67$
i	$p\overline{K^0}$	$\Sigma\eta_s$	-1	$-2f^2_{\Sigma NK}m_{\Sigma\Sigma\eta_s}$	$(D-F)^2$	$+0.29$

TABLE XVI. Indirect sea-quark loop contributions from s valence quarks to the Σ^+ magnetic moment. Here the s-valence quark forms a meson composed with a sea-quark loop as illustrated in Fig. 2. η_s denotes the $s\bar{s}$ η meson.

Diagram	Channel	Mass	Charge	Term	β	χ
e	$p\overline{K^0}$	NK	$+1$	$2f^2_{\Sigma NK}m_{\Sigma NK}$	$-(D-F)^2$	-0.29
f	$p\overline{K^0}$	NK	$+1$	$2f^2_{\Sigma NK}m_{\Sigma NK}$	$-(D-F)^2$	-0.29
i	$p\overline{K^0}$	$\Sigma\,\eta_s$	$+1$	$2f^2_{\Sigma NK}m_{\Sigma\Sigma\,\eta_s}$	$-(D-F)^2$	-0.29

where $I(\eta_u,\eta_d)$ denotes the loop integral of Fig. 4(a) for quark flow diagram Fig. 4(c). For equal η_u and η_d masses one recovers

$$\frac{2}{3}(3F-D)^2\log\left(\frac{m^2}{\Lambda^2}\right), \tag{29}$$

where the leading factor is the standard $NN\eta'$ coupling. Double-hairpin η' contributions to Σ and Ξ baryons may be obtained from Eq. (28) with the appropriate quark-flavor assignments. For example, the factor multiplying the tree level contribution to Ξ^--baryon quark-sector magnetic moments is

$$1-\xi_0\frac{2}{3}\left\{4F^2\log\left(\frac{m^2_{s\bar{s}}}{\Lambda^2}\right)+2\cdot 2F(F-D)\times\frac{m^2_{s\bar{s}}\log\left(\frac{m^2_{s\bar{s}}}{\Lambda^2}\right)-m^2_{\pi}\log\left(\frac{m^2_{\pi}}{\Lambda^2}\right)}{m^2_{s\bar{s}}-m^2_{\pi}}+(F-D)^2\log\left(\frac{m^2_{\pi}}{\Lambda^2}\right)\right\}, \tag{30}$$

where remaining loop-integral factors have been incorporated in

$$\xi_0=\frac{M_0^2}{16\pi^2 f_\pi^2}, \tag{31}$$

with the double hair-pin interaction strength $M_0 \sim 0.75$ GeV [46,47]. While this logarithmic divergence dominates the chiral expansion near the chiral limit, application of these results to the extrapolation of the quenched proton magnetic moment [48] reveals that the curvature associated with this term is small for $m_\pi^2 \gtrsim 0.1$ GeV^2.

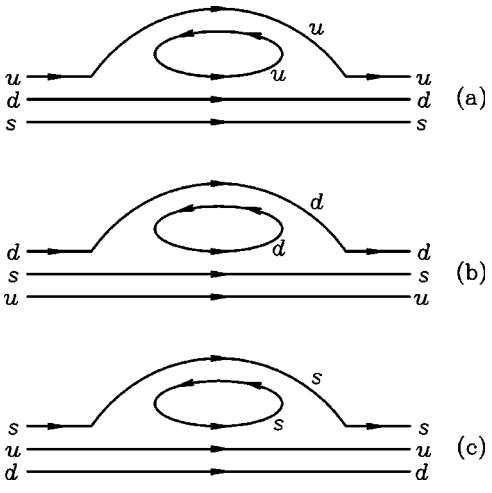

FIG. 3. Key quark-flow diagrams for the Λ baryon. Diagrams (a), (b) and (c) are proportional to the introduced couplings f_u^2, f_d^2 and f_s^2 respectively.

IV. RESULTS

This approach allows one to separate an individual quark-flavor contribution to a baryon form factor into five categories, namely: ''total'' full-QCD contributions, ''direct sea-quark loop,'' and ''valence'' contributions of full-QCD, obtained by removing the direct current coupling to sea-quark loops from the total contributions. Upon further removing ''indirect sea-quark loop'' contributions, one obtains

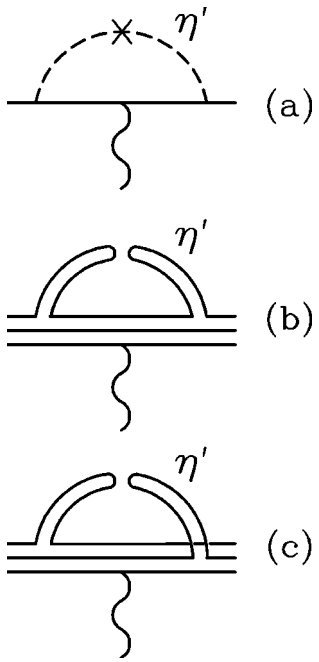

FIG. 4. Diagrams giving rise to the logarithmic divergence of a baryon magnetic moment in the quenched approximation. The cross on the meson propagator in (a) denotes the double hairpin graph of the quark-flow diagrams of (b) and (c).

TABLE XVII. Coefficients, β, providing the LNA contribution to nucleon, Σ and Λ-baryon magnetic moments by quark sectors with quark charges normalized to unit charge. Intermediate (Int.) meson-baryon channels are indicated to allow for $SU(3)$-flavor breaking in both the meson and baryon masses. Total, direct sea-quark loop, valence, indirect sea-quark loop and quenched valence coefficients are indicated.

q	Int.	Total Quark Sector	Direct Sea-Quark Loop	Valence Sector	Indirect Loop	Quenched Valence
u_p	$N\pi$	$-(D+F)^2$	$(5D^2-6DF+9F^2)/3$	$-4(2D^2+3F^2)/3$	$-4(D^2+3F^2)/3$	$-4D^2/3$
	ΛK	$-(D+3F)^2/6$	0	$-(D+3F)^2/6$	$-(D+3F)^2/6$	0
	ΣK	$-(D-F)^2/2$	0	$-(D-F)^2/2$	$-(D-F)^2/2$	0
d_p	$N\pi$	$(D+F)^2$	$(5D^2-6DF+9F^2)/3$	$-2(D^2-6DF+3F^2)/3$	$-2(D-F)^2$	$4D^2/3$
	ΣK	$-(D-F)^2$	0	$-(D-F)^2$	$-(D-F)^2$	0
s_p	ΛK	$(D+3F)^2/6$	$(D+3F)^2/6$	0	0	0
	ΣK	$3(D-F)^2/2$	$3(D-F)^2/2$	0	0	0
u_{Σ^+}	$\Sigma\pi$	$-2F^2$	$2F^2$	$-4F^2$	$-4F^2$	0
	$\Lambda\pi$	$-2D^2/3$	$2D^2/3$	$-4D^2/3$	$-4D^2/3$	0
	NK	0	$(D-F)^2$	$-(D-F)^2$	0	$-(D-F)^2$
	ΞK	$-(D+F)^2$	0	$-(D+F)^2$	$-2(D^2+3F^2)/3$	$-(D^2+6DF-3F^2)/3$
d_{Σ^+}	$\Sigma\pi$	$2F^2$	$2F^2$	0	0	0
	$\Lambda\pi$	$2D^2/3$	$2D^2/3$	0	0	0
	NK	$(D-F)^2$	$(D-F)^2$	0	0	0
s_{Σ^+}	$\Sigma\eta_s$	0	$(D-F)^2$	$-(D-F)^2$	$-(D-F)^2$	0
	NK	$-(D-F)^2$	0	$-(D-F)^2$	$-2(D-F)^2$	$(D-F)^2$
	ΞK	$(D+F)^2$	$2(D^2+3F^2)/3$	$(D^2+6DF-3F^2)/3$	0	$(D^2+6DF-3F^2)/3$
$u_{\Sigma^0}\mid d_{\Sigma^0}$	$\Sigma\pi$	0	$2F^2$	$-2F^2$	$-2F^2$	0
	$\Lambda\pi$	0	$2D^2/3$	$-2D^2/3$	$-2D^2/3$	0
	NK	$(D-F)^2/2$	$(D-F)^2$	$-(D-F)^2/2$	0	$-(D-F)^2/2$
	ΞK	$-(D+F)^2/2$	0	$-(D+F)^2/2$	$-(D^2+3F^2)/3$	$-(D^2+6DF-3F^2)/6$
$u_\Lambda\mid d_\Lambda$	$\Sigma\pi$	0	$2D^2/3$	$-2D^2/3$	$-2D^2/3$	0
	$\Lambda\eta_l$	0	$2(2D-3F)^2/9$	$-2(2D-3F)^2/9$	$-2(2D-3F)^2/9$	0
	NK	$(D+3F)^2/6$	$(D+3F)^2/9$	$(D+3F)^2/18$	0	$(D+3F)^2/18$
	ΞK	$-(D-3F)^2/6$	0	$-(D-3F)^2/6$	$(-7D^2+12DF-9F^2)/9$	$(11D^2-6DF-9F^2)/18$
s_Λ	$\Lambda\eta_s$	0	$(D+3F)^2/9$	$-(D+3F)^2/9$	$-(D+3F)^2/9$	0
	NK	$-(D+3F)^2/3$	0	$-(D+3F)^2/3$	$-2(D+3F)^2/9$	$-(D+3F)^2/9$
	ΞK	$(D-3F)^2/3$	$2(7D^2-12DF+9F^2)/9$	$-(11D^2-6DF-9F^2)/9$	0	$-(11D^2-6DF-9F^2)/9$

the ''quenched valence'' contributions. Tables XVII and XVIII report the axial couplings for these quark-sector contributions to baryon magnetic moments.

The LNA ''direct sea-quark loop'' contribution is relevant to disconnected insertions of the EM current in *either* full or quenched QCD, whereas the LNA ''valence'' contribution is relevant to connected insertions of the EM current only in full QCD. The final category of ''quenched valence'' contributions is relevant to connected insertions of the EM current in quenched QCD. The latter is commonly referred to as the quenched QCD result.

The channels denoted ΩK in Tables XVII, XVIII and in the following actually involve the propagation of an octet *sss* baryon; i.e. the Ξ^- baryon with $m_d=m_s$. In separating valence and sea-quark loop contributions, the cancellation of valence and sea-quark loop octet-*sss*-baryon contributions does not occur. Figure 5 provides quark flow diagrams for $\Xi^0\to\Omega^-K^+$ which illustrate this phenomenon.

In the $SU(3)$-flavor symmetry limit, Figs. 5(a) and (b) are equivalent due to the flavor-blindness of QCD interactions. Figure 5(b) certainly has overlap with an octet-$\Xi^-\pi^+$ intermediate state. Hence the diagram of Fig. 5(a) also has an octet baryon propagating in the intermediate state. Of course, we know there is no *sss* octet baryon and this problem is solved by the contribution of Fig. 5(c) which must be equal but opposite in sign to Fig. 5(a) when an octet baryon propagates in the intermediate state, thus eliminating the octet *sss* baryon contribution in full QCD. In separating valence and sea contributions, each quark flow graph must be taken on its own such that octet baryons are not necessarily eliminated. Indeed, in quenched QCD, only Fig. 5(c) survives, and this quark flow graph has an *sss*-octet baryon propagating in the intermediate state. To some extent this physics has already been seen in Figs. 1(d) plus (e) where only a decuplet baryon can contribute in full QCD, but octet baryons provide contributions in the process of separating valence and sea sectors.

Baryon moments are constructed from the quark sector coefficients by multiplying the *u*, *d* and *s* results by their appropriate charge factors and summing. For example, the proton moment is

$$\mu_p=\frac{2}{3}u_p-\frac{1}{3}d_p-\frac{1}{3}s_p, \tag{32}$$

and the neutron moment is

$$\mu_n=-\frac{1}{3}u_p+\frac{2}{3}d_p-\frac{1}{3}s_p. \tag{33}$$

Similarly, the Σ^+ moment is

$$\mu_{\Sigma^+}=\frac{2}{3}u_{\Sigma^+}-\frac{1}{3}d_{\Sigma^+}-\frac{1}{3}s_{\Sigma^+}, \tag{34}$$

and the Σ^- moment is

TABLE XVIII. Coefficients, β, providing the LNA contribution to Ξ-baryon magnetic moments by quark sectors with quark charges normalized to unit charge. Intermediate (Int.) meson-baryon channels are indicated to allow for $SU(3)$-flavor breaking in both the meson and baryon masses. Total, direct sea-quark loop, valence, indirect sea-quark loop and quenched valence coefficients are indicated.

q	Int.	Total Quark Sector	Direct Sea-Quark Loop	Valence Sector	Indirect Loop	Quenched Valence
u_{Ξ^0}	$\Xi\pi$	$-(D-F)^2$	$(D-F)^2$	$-2(D-F)^2$	$-2(D-F)^2$	0
	ΛK	0	$(D-3F)^2/6$	$-(D-3F)^2/6$	0	$-(D-3F)^2/6$
	ΣK	$(D+F)^2$	$(D+F)^2/2$	$(D+F)^2/2$	0	$(D+F)^2/2$
	ΩK	0	0	0	$-(D-F)^2$	$(D-F)^2$
d_{Ξ^0}	$\Xi\pi$	$(D-F)^2$	$(D-F)^2$	0	0	0
	ΛK	$(D-3F)^2/6$	$(D-3F)^2/6$	0	0	0
	ΣK	$(D+F)^2/2$	$(D+F)^2/2$	0	0	0
s_{Ξ^0}	ΛK	$-(D-3F)^2/6$	0	$-(D-3F)^2/6$	$-(D-3F)^2/3$	$(D-3F)^2/6$
	ΣK	$-3(D+F)^2/2$	0	$-3(D+F)^2/2$	$-(D+F)^2$	$-(D+F)^2/2$
	ΩK	0	$(D-F)^2$	$-(D-F)^2$	0	$-(D-F)^2$
	$\Xi\eta_s$	0	$2(D^2+3F^2)/3$	$-2(D^2+3F^2)/3$	$-2(D^2+3F^2)/3$	0

$$\mu_{\Sigma^-} = -\frac{1}{3}u_{\Sigma^+} + \frac{2}{3}d_{\Sigma^+} - \frac{1}{3}s_{\Sigma^+}. \tag{35}$$

Tables XIX and XX report the axial couplings for the intermediate meson-baryon channels contributing to the nonanalytic behavior of baryon magnetic moments. We note that upon neglecting the baryon mass splittings, one recovers the full QCD results of Ref. [34] summarized in their Eqs. (A.2) and (A.4), and the quenched results of Ref. [28] summarized in their Table 2.

Table XXI reports values for the coefficient, χ, providingthe LNA contribution to baryon magnetic moments (χm_π or χm_K or χm_{η_s} as appropriate) by quark sectors with each quark flavor normalized to unit charge. Charge symmetry provides the contributions for other baryons. Values are based on the tree-level axial couplings $F=0.50$ and $D=0.76$ with $f_\pi=93$ MeV. Similar results for bulk baryon moments are provided in Table XXII. For convenience, values using the one-loop corrected values [34] of $F=0.40$ and $D=0.61$ are provided in Tables XXIII and XXIV respectively.

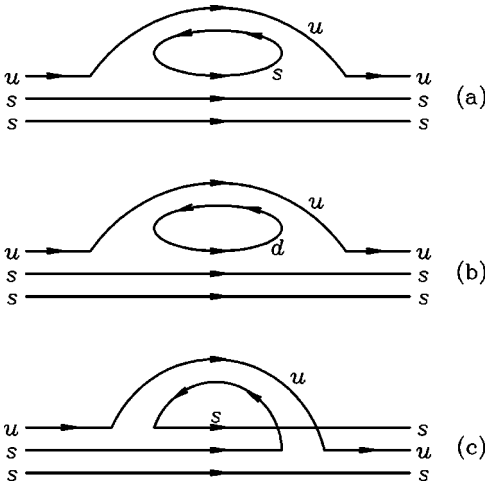

FIG. 5. Quark-flow diagrams illustrating the presence of an *sss*-octet baryon propagating in each of diagrams (a) and (c). Further discussion is provided in the text.

V. PARTIAL QUENCHING

A. Hadron masses

The flavor-blind nature of QCD makes it trivial to extend this calculation of quenched baryon magnetic moments to the partially quenched theory. As new flavors are introduced through the use of dynamically generated gauge fields, one simply adds the direct and indirect sea-quark loop contributions evaluated in Sec. III to the quenched results of Sec. IV. To incorporate hadron mass violations of $SU(3)$-flavor symmetry, one must track the meson mass of the valence-sea meson. As we have already isolated each valence quark flavor contribution to the baryon moment, the mass of the meson is identified by the valence- and sea-quark mass composing the meson.

It should be noted that the double hair-pin graph of the η' meson remains anomalous in the partially quenched theory [49]. However, the contribution of the η' propagator is suppressed by the difference in valence- and sea-quark masses.

B. Sea- and ghost-quark electric charge assignments

There has been some discussion on the electric charge assignments that may be applied to the various quark sectors of partially quenched effective field theory [29]. In the conventional view of quenched chiral perturbation theory, the charges of the commuting ghost-quark fields are tied to the valence quark charges in order to eliminate both the direct and indirect sea-quark loop contributions of the valence sector. Similarly, for partially quenched chiral perturbation theory, it is usually argued that the ghost quarks are identical to the valence quarks, except for their statistics.

However, it has been indicated that when the number of sea quarks matches the number of valence quarks, more general charge assignments are possible [29]. The idea is that when the masses and charges of the sea- and ghost-quarks

TABLE XIX. Coefficients, β, providing the LNA contribution to nucleon magnetic moments. Intermediate (Int.) meson-baryon channels are indicated to allow for $SU(3)$-flavor breaking in both the meson and baryon masses.

Baryon	Int.	Total Quark Sector	Direct Sea-Quark Loop	Valence Sector	Indirect Loop	Quenched Valence
p	$N\pi$	$-(D+F)^2$	$(5D^2-6DF+9F^2)/9$	$2(-7D^2-6DF-9F^2)/9$	$-2(D+3F)^2/9$	$-4D^2/3$
	ΛK	$-(D+3F)^2/6$	$-(D+3F)^2/18$	$-(D+3F)^2/9$	$-(D+3F)^2/9$	0
	ΣK	$-(D-F)^2/2$	$-(D-F)^2/2$	0	0	0
n	$N\pi$	$(D+F)^2$	$(5D^2-6DF+9F^2)/9$	$4D(D+6F)/9$	$8D(-D+3F)/9$	$4D^2/3$
	ΛK	0	$-(D+3F)^2/18$	$(D+3F)^2/18$	$(D+3F)^2/18$	0
	ΣK	$-(D-F)^2$	$-(D-F)^2/2$	$-(D-F)^2/2$	$-(D-F)^2/2$	0

match, these contributions cancel leaving the theory of full QCD. In this case the charges of the sea and ghost quarks need not be related to the valence quarks. However, it is essential that the quark masses of the valence and ghost sectors match, such that the indirect sea-quark loop contributions of the valence sector continue to be quenched.

We have already argued in the Introduction that it is important to provide an opportunity to include disconnected insertions of the electromagnetic current in the quenched approximation. These insertions can be calculated in the quenched approximation and give rise to direct sea-quark loop contributions. It is now clear that this goal can be realized in the formal theory of quenched chiral perturbation theory by assigning neutral electric charges to the ghost-quark fields. Indirect sea-quark loop contributions are removed while leaving direct sea-quark loop contributions from the valence sector unaltered.

C. Examples

Consider for example the quark sector contributions to a baryon magnetic moment in a partially quenched theory with two degenerate light quarks and one heavy sea quark, labeled u', d' and s'. Electric charge assignments are q_u, q_d, q_s for the valence sector of the theory and q'_u, q'_d, q'_s for the ghost- and sea-quark sectors.

1. Proton magnetic moment

The quenched quark-sector results for the proton are complemented by direct sea-quark loop contributions from the valence- and ghost-quark sectors plus both direct and indirect contributions from the sea-quark sector. As discussed in Sec. III A such loop contributions are flavor blind and the couplings are easily extracted from Tables IV, VII or IX for the direct contributions and Table V for the indirect contribution. For simplicity, we will suppress baryon mass splittings in the following. However, they may be introduced in a transparent manner.

For the u-quark sector in the proton, one has

$$u_p=\xi\Big\{-q_u\frac{4}{3}D^2m_\pi+q_u\frac{1}{3}(5D^2-6DF+9F^2)m_\pi + q'_u\frac{1}{3}(5D^2-6DF+9F^2)(\tilde{m}_\pi-m_\pi) - q_u\frac{4}{3}(D^2+3F^2)\tilde{m}_\pi-q_u\frac{2}{3}(D^2+3F^2)\tilde{m}_K\Big\}, \quad (36)$$

where $\xi\equiv m_N/(8\pi f_\pi^2)$. $\tilde{m}_\pi$ denotes a π-meson composed of a light-valence and light-sea quark, and $\tilde{m}_K$ denotes a K-meson composed of a light-valence and heavy-sea quark. The second term is a direct u sea-quark loop contribution associated with the valence sector, canceled by the ghost-quark contribution in the third term when $q'_u=q_u$. The third term also includes the direct u' sea-quark loop contribution associated with the sea-quark sector and originates from Table IV for Figs. 1(b) and (e). The last two terms are indirect u sea-quark loop contributions and originate from Table V for diagrams (b), (g) and (h) respectively.

Similarly

$$d_p=\xi\Big\{+q_d\frac{4}{3}D^2m_\pi+q_d\frac{1}{3}(5D^2-6DF+9F^2)m_\pi + q'_d\frac{1}{3}(5D^2-6DF+9F^2)(\tilde{m}_\pi-m_\pi) - q_d2(D-F)^2\tilde{m}_\pi-q_d(D-F)^2\tilde{m}_K\Big\}, \quad (37)$$

and

$$s_p=\xi\Big\{q_s\frac{1}{3}(5D^2-6DF+9F^2)m_K + q'_s\frac{1}{3}(5D^2-6DF+9F^2)(\tilde{m}_K-m_K)\Big\}. \quad (38)$$

The LNA behavior of the proton magnetic moment in the partially quenched theory is

$$\mu_p=\xi\Big\{-\frac{4}{3}D^2m_\pi+\frac{1}{9}(5D^2-6DF+9F^2)(m_\pi-m_K) + (q'_u+q'_d)\frac{1}{3}(5D^2-6DF+9F^2)(\tilde{m}_\pi-m_\pi) + q'_s\frac{1}{3}(5D^2-6DF+9F^2)(\tilde{m}_K-m_K) - \frac{2}{9}(D+3F)^2\tilde{m}_\pi-\frac{1}{9}(D+3F)^2\tilde{m}_K\Big\}. \quad (39)$$

TABLE XX. Coefficients, β, providing the LNA contribution to Σ-, Λ- and Ξ-baryon magnetic moments. Intermediate (Int.) meson-baryon channels are indicated to allow for $SU(3)$-flavor breaking in both the meson and baryon masses.

Baryon	Int.	Total Quark Sector	Direct Sea-Quark Loop	Valence Sector	Indirect Loop	Quenched Valence
Σ^+	$\Sigma\pi$	$-2F^2$	$2F^2/3$	$-8F^2/3$	$-8F^2/3$	0
	$\Lambda\pi$	$-2D^2/3$	$2D^2/9$	$-8D^2/9$	$-8D^2/9$	0
	NK	0	$(D-F)^2/3$	$-(D-F)^2/3$	$2(D-F)^2/3$	$-(D-F)^2$
	ΞK	$-(D+F)^2$	$-2(D^2+3F^2)/9$	$(-7D^2-18DF-3F^2)/9$	$-4(D^2+3F^2)/9$	$-(D^2+6DF-3F^2)/3$
	$\Sigma\eta_s$	0	$-(D-F)^2/3$	$(D-F)^2/3$	$(D-F)^2/3$	0
Σ^0	$\Sigma\pi$	0	$2F^2/3$	$-2F^2/3$	$-2F^2/3$	0
	$\Lambda\pi$	0	$2D^2/9$	$-2D^2/9$	$-2D^2/9$	0
	NK	$(D-F)^2/2$	$(D-F)^2/3$	$(D-F)^2/6$	$2(D-F)^2/3$	$-(D-F)^2/2$
	ΞK	$-(D+F)^2/2$	$-2(D^2+3F^2)/9$	$(-5D^2-18DF+3F^2)/18$	$-(D^2+3F^2)/9$	$-(D^2+6DF-3F^2)/6$
	$\Sigma\eta_s$	0	$-(D-F)^2/3$	$(D-F)^2/3$	$(D-F)^2/3$	0
Σ^-	$\Sigma\pi$	$2F^2$	$2F^2/3$	$4F^2/3$	$4F^2/3$	0
	$\Lambda\pi$	$2D^2/3$	$2D^2/9$	$4D^2/9$	$4D^2/9$	0
	NK	$(D-F)^2$	$(D-F)^2/3$	$2(D-F)^2/3$	$2(D-F)^2/3$	$-(D-F)^2$
	ΞK	0	$-2(D^2+3F^2)/9$	$2(D^2+3F^2)/9$	$2(D^2+3F^2)/9$	0
	$\Sigma\eta_s$	0	$-(D-F)^2/3$	$(D-F)^2/3$	$(D-F)^2/3$	0
Λ	$\Sigma\pi$	0	$2D^2/9$	$-2D^2/9$	$-2D^2/9$	0
	$\Lambda\eta_l$	0	$2(2D-3F)^2/27$	$-2(2D-3F)^2/27$	$-2(2D-3F)^2/27$	0
	NK	$(D+3F)^2/6$	$(D+3F)^2/27$	$7(D+3F)^2/54$	$2(D+3F)^2/27$	$(D+3F)^2/18$
	ΞK	$-(D-3F)^2/6$	$2(-7D^2+12DF-9F^2)/27$	$(19D^2+6DF-45F^2)/54$	$(-7D^2+12DF-9F^2)/27$	$(11D^2-6DF-9F^2)/18$
	$\Lambda\eta_s$	0	$-(D+3F)^2/27$	$(D+3F)^2/27$	$(D+3F)^2/27$	0
Ξ^0	$\Xi\pi$	$-(D-F)^2$	$(D-F)^2/3$	$-4(D-F)^2/3$	$-4(D-F)^2/3$	0
	ΛK	0	$(D-3F)^2/18$	$-(D-3F)^2/18$	$(D-3F)^2/9$	$-(D-3F)^2/6$
	ΣK	$(D+F)^2$	$(D+F)^2/6$	$5(D+F)^2/6$	$(D+F)^2/3$	$(D+F)^2/2$
	ΩK	0	$-(D-F)^2/3$	$(D-F)^2/3$	$-2(D-F)^2/3$	$(D-F)^2$
	$\Xi\eta_s$	0	$-2(D^2+3F^2)/9$	$2(D^2+3F^2)/9$	$2(D^2+3F^2)/9$	0
Ξ^-	$\Xi\pi$	$(D-F)^2$	$(D-F)^2/3$	$2(D-F)^2/3$	$2(D-F)^2/3$	0
	ΛK	$(D-3F)^2/6$	$(D-3F)^2/18$	$(D-3F)^2/9$	$(D-3F)^2/9$	0
	ΣK	$(D+F)^2/2$	$(D+F)^2/6$	$(D+F)^2/3$	$(D+F)^2/3$	0
	ΩK	0	$-(D-F)^2/3$	$(D-F)^2/3$	$(D-F)^2/3$	0
	$\Xi\eta_s$	0	$-2(D^2+3F^2)/9$	$2(D^2+3F^2)/9$	$2(D^2+3F^2)/9$	0

We note that this final expression agrees with that of Eq. (48) in Ref. [29].

2. Σ^+ *magnetic moment*

To clearly establish the method for constructing partially quenched chiral coefficients, we consider the Σ^+ hyperon. The direct and indirect sea-quark loop contributions are flavor blind and the couplings are easily extracted from Tables XI, XIII or XV for the direct contributions and Table XII for the indirect contribution. For the u-quark sector in Σ^+, one has

$$u_{\Sigma^+}=\xi\Big\{-q_u\frac{4}{3}D^2m_K+q_u\frac{2}{3}(D^2+3F^2)m_\pi+q_u(D-F)^2m_K+q_u'\frac{2}{3}(D^2+3F^2)(\tilde{m}_\pi-m_\pi)+q_u'(D-F)^2(\hat{m}_K-m_K)-q_u\frac{4}{3}(D^2+3F^2)\tilde{m}_\pi-q_u\frac{2}{3}(D^2+3F^2)\tilde{m}_K\Big\},\tag{40}$$

where $\tilde{m}_K$ denotes a K-meson composed of a light-valence and heavy-sea quark and $\hat{m}_K$ denotes a K-meson composed of a strange-valence and light-sea quark. The second and third terms are direct u sea-quark loop contributions associated with the valence sector, canceled by the ghost-quark contribution in the fourth and fifth terms when $q_u'=q_u$. The fourth and fifth terms also include the direct u' sea-quark loop contribution associated with the sea-quark sector and originate from Table XI for Figs. 2(b) and (e). The last two terms are indirect u sea-quark loop contributions and originate from Table XII for Figs. 2(b)+(c) and (h) respectively. Similarly

$$s_{\Sigma^+}=\xi\Big\{+q_s\frac{4}{3}D^2m_K+q_s\frac{2}{3}(D^2+3F^2)m_K+q_s(D-F)^2m_{\eta_s}+q_s'\frac{2}{3}(D^2+3F^2)(\tilde{m}_K-m_K)+q_s'(D-F)^2\times(\tilde{m}_{\eta_s}-m_{\eta_s})-q_s2(D-F)^2\hat{m}_K-q_s(D-F)^2\tilde{m}_{\eta_s}\Big\},\tag{41}$$

where $\tilde{m}_{\eta_s}$ denotes an $s\overline{s'}$ η-meson composed of a strange-valence and antiheavy sea-quark, and

$$d_{\Sigma^+}=\xi\Big\{+q_d\frac{2}{3}(D^2+3F^2)m_\pi+q_d(D-F)^2m_K+q_d'\frac{2}{3}(D^2+3F^2)(\tilde{m}_\pi-m_\pi)+q_d'(D-F)^2(\hat{m}_K-m_K)\Big\}.\tag{42}$$

Thus, the LNA behavior of the Σ^+ magnetic moment in the partially quenched theory is

$$\begin{aligned}\mu_{\Sigma^+} = \xi\Big\{ & -\frac{4}{3}D^2 m_K + \frac{2}{9}(D^2+3F^2)m_\pi + \frac{1}{3}(D-F)^2 m_K \\ & -\frac{2}{9}(D^2+3F^2)m_K - \frac{1}{3}(D-F)^2 m_{\eta_s} \\ & +(q'_u+q'_d)\frac{2}{3}(D^2+3F^2)(\tilde{m}_\pi - m_\pi) \\ & +(q'_u+q'_d)(D-F)^2(\hat{m}_K - m_K) \\ & +q'_s\frac{2}{3}(D^2+3F^2)(\tilde{m}_K - m_K) \\ & +q'_s(D-F)^2(\tilde{m}_{\eta_s} - m_{\eta_s}) + \frac{1}{3}(D-F)^2(2\hat{m}_K + \tilde{m}_{\eta_s}) \\ & -\frac{4}{9}(D^2+3F^2)(2\tilde{m}_\pi + \tilde{m}_K)\Big\}, \end{aligned} \tag{43}$$

again in agreement with Eq. (51) of Ref. [29].

Partially quenched results may be similarly obtained for the remainder of the quark-sector contributions to octet baryon magnetic moments using the approach described here in detail. Since the results require specific knowledge of the number and nature of dynamical flavors, we defer writing further specific results.

VI. SUMMARY

The diagrammatic method for separating valence and sea-quark-loop contributions to the meson cloud of hadrons provides a transparent approach to the calculation of quenched chiral coefficients. The origin of chiral nonanalytic structure is obvious, and facilitates the incorporation of the correct nonanalytic structure matching today's numerical simulations. In the process, the coefficients for partially quenched QCD are derived; no new calculations are required.

The valence sector of full QCD contains the largest coefficients for the leading nonanalytic behavior of magnetic moments. The *u*-quark contribution to the proton magnetic moment has a coefficient of -11.0 for the rapidly varying pion-cloud contribution, which is complemented further by the kaon cloud. These are connected insertions of the electromagnetic current in full QCD and should reveal significant curvature in the approach to the chiral limit. It is also encouraging to note that the *u*-quark sector is known to have relatively small statistical uncertainties in the quenched approximation [35] compared to that for the *d* quark.

The coefficients of the leading nonanalytic terms of full QCD change significantly upon quenching. Some channels still hold excellent promise for revealing the nonanalytic behavior of meson-cloud physics even in the quenched approximation. For example, the *u* or *d*-quark in the proton have large coefficients for the nonanalytic term proportional to m_π, with opposite signs respectively. Similarly, both the proton and neutron magnetic moments have large coefficients surviving in quenched QCD. Because the *u*-quark in the proton has significantly smaller statistical errors than that for the *d* quark in the proton [35], the *u*-quark contribution to the proton magnetic moment provides the optimal opportunity to directly view nonanalytic behavior associated with the quenched meson cloud of baryons in the quenched approximation. Figure 6 illustrates the anticipated curvature [2] associated with the term $-(4/3)D^2 m_N m_\pi/(8\pi f_\pi^2)$ surviving in the quenched approximation.

There are other interesting opportunities. Consider for example the *s*-quark contribution to the quenched Λ magnetic moment. Table XXI indicates that the coefficient of the *NK* contribution to the Λ magnetic moment is large. Because the nucleon is significantly lighter than the Λ, the *NK* loop can contribute enhanced nonlinear behavior. Hence, there is a prediction of significant curvature in the extrapolation of the *s*-quark contribution, even when the mass of the strange quark is held fixed as is commonly done in lattice QCD simulations. As such, the effect is purely environmental [35,36,39,40].

The effect arises from the extrapolation of light *u* and *d* quarks in the Λ.

The *s*-quark in Ξ provides another opportunity to observe a purely environmental effect in quenched QCD. Here the coefficient of the ΣK channel is very large, again predicting curvature in the *s*-quark contribution to the magnetic moment, even when the *s*-quark mass is held fixed. The mass of Σ is less than the mass of Ξ allowing the kaon to provide enhanced nonlinear behavior.

A few channels hold potential for revealing *quenched artifacts* in quenched simulations. Despite the prediction of curvature for both the *s* and *d*-quark sectors of Ξ^- in both full and quenched QCD, the extrapolation of the total Ξ^--baryon magnetic moment receives no leading nonanalytic contribution from either the π- or the *K*-meson cloud in the quenched approximation. Similar results hold for the Σ^- magnetic moment.

It is particularly difficult to directly determine the loop contribution to baryon magnetic moments in numerical simulations [30–33]. As such, it is of particular interest to compare the coefficients of the valence quark contributions in full QCD (column ''valence'' of Tables XXI and XXII) to that for the valence quark contributions of quenched QCD (column ''quenched valence'' of Tables XXI and XXII). Here, the *u*-quark in Σ^+ stands out with the significant curvature of the $\Sigma\pi$ and $\Lambda\pi$ channels completely suppressed from -4.32 to 0 and -3.33 to 0 respectively. Only the ΞK channel has a significant coupling for the *u* quark in the quenched Σ^+, but curvature in this channel is suppressed by the large excitation energy required to form the intermediate state. The *u* quark in the proton is also worthy of note, with the coefficient of the rapidly varying πN channel dropping significantly from -11.0 in full QCD to -3.33 in quenched QCD and the kaon contribution vanishing completely.

TABLE XXI. Coefficients, χ, providing the LNA contribution to baryon magnetic moments by quark sectors with quark charges normalized to unit charge. Intermediate (Int.) meson-baryon channels are indicated to allow for $SU(3)$-flavor breaking in both the meson and baryon masses. Total, direct sea-quark loop (direct loop), valence, indirect sea-quark loop (indirect loop) and quenched valence coefficients are indicated. The axial couplings take the tree-level values $F=0.50$ and $D=0.76$ with $f_\pi=93$ MeV. Note $\epsilon=0.0004$.

q	Int.	Total	Direct Loop	Valence	Indirect Loop	Quenched Valence
u_p	$N\pi$	-6.87	$+4.12$	-11.0	-7.65	-3.33
	ΛK	-3.68	0	-3.68	-3.68	0
	ΣK	-0.15	0	-0.15	-0.15	0
d_p	$N\pi$	$+6.87$	$+4.12$	$+2.75$	-0.59	$+3.33$
	ΣK	-0.29	0	-0.29	-0.29	0
s_p	ΛK	$+3.68$	$+3.68$	0	0	0
	ΣK	$+0.44$	$+0.44$	0	0	0
u_{Σ^+}	$\Sigma\pi$	-2.16	$+2.16$	-4.32	-4.32	0
	$\Lambda\pi$	-1.67	$+1.67$	-3.33	-3.33	0
	NK	0	$+0.29$	-0.29	0	-0.29
	ΞK	-6.87	0	-6.87	-3.83	-3.04
d_{Σ^+}	$\Sigma\pi$	$+2.16$	$+2.16$	0	0	0
	$\Lambda\pi$	$+1.67$	$+1.67$	0	0	0
	NK	$+0.29$	$+0.29$	0	0	0
s_{Σ^+}	NK	-0.29	0	-0.29	-0.59	$+0.29$
	ΞK	$+6.87$	$+3.83$	$+3.04$	0	$+3.04$
	$\Sigma\eta_s$	0	$+0.29$	-0.29	-0.29	0
$u_{\Sigma^0}\vert d_{\Sigma^0}$	$\Sigma\pi$	0	$+2.16$	-2.16	-2.16	0
	$\Lambda\pi$	0	$+1.67$	-1.67	-1.67	0
	NK	$+0.15$	$+0.29$	-0.15	0	-0.15
	ΞK	-3.43	0	-3.43	-1.91	-1.52
$u_\Lambda\vert d_\Lambda$	$\Sigma\pi$	0	$+1.67$	-1.67	-1.67	0
	$\Lambda\eta_l$	0	ϵ	$-\epsilon$	$-\epsilon$	0
	NK	$+3.68$	$+2.45$	$+1.23$	0	$+1.23$
	ΞK	-0.40	0	-0.40	-0.83	$+0.44$
s_Λ	$\Lambda\eta_s$	0	$+2.45$	-2.45	-2.45	0
	NK	-7.36	0	-7.36	-4.91	-2.45
	ΞK	$+0.79$	$+1.67$	-0.88	0	-0.88
u_{Ξ^0}	$\Xi\pi$	-0.29	$+0.29$	-0.59	-0.59	0
	ΛK	0	$+0.40$	-0.40	0	-0.40
	ΣK	$+6.87$	$+3.43$	$+3.43$	0	$+3.43$
	ΩK	0	0	0	-0.29	$+0.29$
d_{Ξ^0}	$\Xi\pi$	$+0.29$	$+0.29$	0	0	0
	ΛK	$+0.40$	$+0.40$	0	0	0
	ΣK	$+3.43$	$+3.43$	0	0	0
s_{Ξ^0}	ΛK	-0.40	0	-0.40	-0.79	$+0.40$
	ΣK	-10.3	0	-10.3	-6.87	-3.43
	ΩK	0	$+0.29$	-0.29	0	-0.29
	$\Xi\eta_s$	0	$+3.83$	-3.83	-3.83	0

TABLE XXII. Coefficients, χ, providing the LNA contribution to baryon magnetic moments. Intermediate (Int.) meson-baryon channels are indicated to allow for $SU(3)$-flavor breaking in both the meson and baryon masses. Total, direct sea-quark loop (direct loop), valence, indirect sea-quark loop (indirect loop) and quenched valence coefficients are indicated. The axial couplings take the tree-level values $F=0.50$ and $D=0.76$ with $f_\pi=93$ MeV. Note $\epsilon=0.0001$.

Baryon	Channel	Total	Direct Loop	Valence	Indirect Loop	Quenched Valence
p	$N\pi$	-6.87	$+1.37$	-8.24	-4.91	-3.33
	ΛK	-3.68	-1.23	-2.45	-2.45	0
	ΣK	-0.15	-0.15	0	0	0
n	$N\pi$	$+6.87$	$+1.37$	$+5.49$	$+2.16$	$+3.33$
	ΛK	0	-1.23	$+1.23$	$+1.23$	0
	ΣK	-0.29	-0.15	-0.15	-0.15	0
Σ^+	$\Sigma\pi$	-2.16	$+0.72$	-2.88	-2.88	0
	$\Lambda\pi$	-1.67	$+0.56$	-2.22	-2.22	0
	NK	0	$+0.10$	-0.10	$+0.20$	-0.29
	ΞK	-6.87	-1.28	-5.59	-2.55	-3.04
	$\Sigma\eta_s$	0	-0.10	$+0.10$	$+0.10$	0
Σ^0	$\Sigma\pi$	0	$+0.72$	-0.72	-0.72	0
	$\Lambda\pi$	0	$+0.56$	-0.56	-0.56	0
	NK	$+0.15$	$+0.10$	$+0.05$	$+0.20$	-0.15
	ΞK	-3.43	-1.28	-2.16	-0.64	-1.52
	$\Sigma\eta_s$	0	-0.10	$+0.10$	$+0.10$	0
Σ^-	$\Sigma\pi$	$+2.16$	$+0.72$	$+1.44$	$+1.44$	0
	$\Lambda\pi$	$+1.67$	$+0.56$	$+1.11$	$+1.11$	0
	NK	$+0.29$	$+0.10$	$+0.20$	$+0.20$	0
	ΞK	0	-1.28	$+1.28$	$+1.28$	0
	$\Sigma\eta_s$	0	-0.10	$+0.10$	$+0.10$	0
Λ	$\Sigma\pi$	0	$+0.56$	-0.56	-0.56	0
	$\Lambda\eta_l$	0	ϵ	$-\epsilon$	$-\epsilon$	0
	NK	$+3.68$	$+0.82$	$+2.86$	$+1.64$	$+1.23$
	ΞK	-0.40	-0.56	$+0.16$	-0.28	$+0.44$
	$\Lambda\eta_s$	0	-0.82	$+0.82$	$+0.82$	0
Ξ^0	$\Xi\pi$	-0.29	$+0.10$	-0.39	-0.39	0
	ΛK	0	$+0.13$	-0.13	$+0.26$	-0.40
	ΣK	$+6.87$	$+1.14$	$+5.72$	$+2.29$	$+3.43$
	ΩK	0	-0.10	$+0.10$	-0.20	$+0.29$
	$\Xi\eta_s$	0	-1.28	$+1.28$	$+1.28$	0
Ξ^-	$\Xi\pi$	$+0.29$	$+0.10$	$+0.20$	$+0.20$	0
	ΛK	$+0.40$	$+0.13$	$+0.26$	$+0.26$	0
	ΣK	$+3.43$	$+1.14$	$+2.29$	$+2.29$	0
	ΩK	0	-0.10	$+0.10$	$+0.10$	0
	$\Xi\eta_s$	0	-1.28	$+1.28$	$+1.28$	0

TABLE XXIII. One-loop corrected coefficients, χ, providing the LNA contribution to baryon magnetic moments by quark sectors with quark charges normalized to unit charge. Total, direct sea-quark loop (direct loop), valence, indirect sea-quark loop (indirect loop) and quenched valence coefficients are indicated. Here, the axial couplings take the one-loop corrected values $F=0.40$ and $D=0.61$ with $f_\pi=93$ MeV. Note $\epsilon=0.0004$.

q	Int.	Total	Direct Loop	Valence	Indirect Loop	Quenched Valence
u_p	$N\pi$	-4.41	$+2.65$	-7.06	-4.91	-2.15
	ΛK	-2.36	0	-2.36	-2.36	0
	ΣK	-0.10	0	-0.10	-0.10	0
d_p	$N\pi$	$+4.41$	$+2.65$	$+1.76$	-0.38	$+2.15$
	ΣK	-0.19	0	-0.19	-0.19	0
s_p	ΛK	$+2.36$	$+2.36$	0	0	0
	ΣK	$+0.29$	$+0.29$	0	0	0
u_{Σ^+}	$\Sigma\pi$	-1.38	$+1.38$	-2.77	-2.77	0
	$\Lambda\pi$	-1.07	$+1.07$	-2.15	-2.15	0
	NK	0	$+0.19$	-0.19	0	-0.19
	ΞK	-4.41	0	-4.41	-2.46	-1.95
d_{Σ^+}	$\Sigma\pi$	$+1.38$	$+1.38$	0	0	0
	$\Lambda\pi$	$+1.07$	$+1.07$	0	0	0
	NK	$+0.19$	$+0.19$	0	0	0
s_{Σ^+}	NK	-0.19	0	-0.19	-0.38	$+0.19$
	ΞK	$+4.41$	$+2.46$	$+1.95$	0	$+1.95$
	$\Sigma\eta_s$	0	$+0.19$	-0.19	-0.19	0
$u_{\Sigma^0}\vert d_{\Sigma^0}$	$\Sigma\pi$	0	$+1.38$	-1.38	-1.38	0
	$\Lambda\pi$	0	$+1.07$	-1.07	-1.07	0
	NK	$+0.10$	$+0.19$	-0.10	0	-0.10
	ΞK	-2.21	0	-2.21	-1.23	-0.98
$u_\Lambda\vert d_\Lambda$	$\Sigma\pi$	0	$+1.07$	-1.07	-1.07	0
	$\Lambda\eta_l$	0	ϵ	$-\epsilon$	$-\epsilon$	0
	NK	$+2.36$	$+1.57$	$+0.79$	0	$+0.79$
	ΞK	-0.25	0	-0.25	-0.54	$+0.29$
s_Λ	$\Lambda\eta_s$	0	$+1.57$	-1.57	-1.57	0
	NK	-4.72	0	-4.72	-3.15	-1.57
	ΞK	$+0.50$	$+1.07$	-0.57	0	-0.57
u_{Ξ^0}	$\Xi\pi$	-0.19	$+0.19$	-0.38	-0.38	0
	ΛK	0	$+0.25$	-0.25	0	-0.25
	ΣK	$+4.41$	$+2.21$	$+2.21$	0	$+2.21$
	ΩK	0	0	0	-0.19	$+0.19$
d_{Ξ^0}	$\Xi\pi$	$+0.19$	$+0.19$	0	0	0
	ΛK	$+0.25$	$+0.25$	0	0	0
	ΣK	$+2.21$	$+2.21$	0	0	0
s_{Ξ^0}	ΛK	-0.25	0	-0.25	-0.50	$+0.25$
	ΣK	-6.62	0	-6.62	-4.41	-2.21
	ΩK	0	$+0.19$	-0.19	0	-0.19
	$\Xi\eta_s$	0	$+2.46$	-2.46	-2.46	0

TABLE XXIV. One-loop corrected coefficients, χ, providing the LNA contribution to baryon magnetic moments. Total, direct sea-quark loop (direct loop), valence, indirect sea-quark loop (indirect loop) and quenched valence coefficients are indicated. Here, the axial couplings take the one-loop corrected values $F=0.40$ and $D=0.61$ with $f_\pi=93$ MeV. Note $\epsilon=0.000128$.

Baryon	Channel	Total	Direct Loop	Valence	Indirect Loop	Quenched Valence
p	$N\pi$	-4.41	$+0.88$	-5.29	-3.15	-2.15
	ΛK	-2.36	-0.79	-1.57	-1.57	0
	ΣK	-0.10	-0.10	0	0	0
n	$N\pi$	$+4.41$	$+0.88$	$+3.53$	$+1.38$	$+2.15$
	ΛK	0	-0.79	$+0.79$	$+0.79$	0
	ΣK	-0.19	-0.10	-0.10	-0.10	0
Σ^+	$\Sigma\pi$	-1.38	$+0.46$	-1.85	-1.85	0
	$\Lambda\pi$	-1.07	$+0.36$	-1.43	-1.43	0
	NK	0	$+0.06$	-0.06	$+0.13$	-0.19
	ΞK	-4.41	-0.82	-3.59	-1.64	-1.95
	$\Sigma\eta_s$	0	-0.06	$+0.06$	$+0.06$	0
Σ^0	$\Sigma\pi$	0	$+0.46$	-0.46	-0.46	0
	$\Lambda\pi$	0	$+0.36$	-0.36	-0.36	0
	NK	$+0.10$	$+0.06$	$+0.03$	$+0.13$	-0.10
	ΞK	-2.21	-0.82	-1.39	-0.41	-0.98
	$\Sigma\eta_s$	0	-0.06	$+0.06$	$+0.06$	0
Σ^-	$\Sigma\pi$	$+1.38$	$+0.46$	$+0.92$	$+0.92$	0
	$\Lambda\pi$	$+1.07$	$+0.36$	$+0.72$	$+0.72$	0
	NK	$+0.19$	$+0.06$	$+0.13$	$+0.13$	0
	ΞK	0	-0.82	$+0.82$	$+0.82$	0
	$\Sigma\eta_s$	0	-0.06	$+0.06$	$+0.06$	0
Λ	$\Sigma\pi$	0	$+0.36$	-0.36	-0.36	0
	$\Lambda\eta_l$	0	ϵ	$-\epsilon$	$-\epsilon$	0
	NK	$+2.36$	$+0.53$	$+1.84$	$+1.05$	$+0.79$
	ΞK	-0.25	-0.36	$+0.11$	-0.18	$+0.29$
	$\Lambda\eta_s$	0	-0.53	$+0.53$	$+0.53$	0
Ξ^0	$\Xi\pi$	-0.19	$+0.06$	-0.25	-0.25	0
	ΛK	0	$+0.08$	-0.08	$+0.17$	-0.25
	ΣK	$+4.41$	$+0.74$	$+3.68$	$+1.47$	$+2.21$
	ΩK	0	-0.06	$+0.06$	-0.13	$+0.19$
	$\Xi\eta_s$	0	-0.82	$+0.82$	$+0.82$	0
Ξ^-	$\Xi\pi$	$+0.19$	$+0.06$	$+0.13$	$+0.13$	0
	ΛK	$+0.25$	$+0.08$	$+0.17$	$+0.17$	0
	ΣK	$+2.21$	$+0.74$	$+1.47$	$+1.47$	0
	ΩK	0	-0.06	$+0.06$	$+0.06$	0
	$\Xi\eta_s$	0	-0.82	$+0.82$	$+0.82$	0

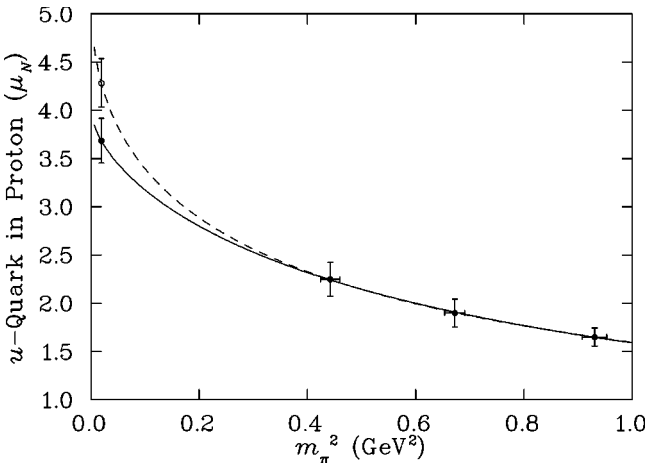

FIG. 6. Chiral extrapolation via the Padé approximation of [2,6]. The solid curve displays the self-consistent extrapolation of the quenched simulation results of [35], whereas the dashed curve shows the curvature of full QCD. One-loop corrected axial couplings are used in the Padé approximation.

In summary, this study of quark-sector contributions to baryon magnetic moments in quenched, partially quenched and full QCD indicates there are numerous opportunities to observe and understand the underlying structure of baryons and the nature of chiral nonanalytic behavior in QCD and its quenched variants. Numerical simulations of the observables discussed herein are currently in production on the Australian Partnership for Advanced Computing (APAC) National Facility using FLIC fermions [18] which provide efficient access to the light quark-mass regime. It will be interesting to confront these predictions with numerical simulation results.

ACKNOWLEDGMENTS

Thanks to Matthias Burkardt, Ian Cloet, Ben Crouch, Martin Savage, Tony Thomas, Tony Williams, Stewart Wright and Ross Young for beneficial discussions. This research is supported by the Australian Research Council.

[1] D.B. Leinweber and T.D. Cohen, Phys. Rev. D **47**, 2147 (1993).
[2] D.B. Leinweber, D.H. Lu, and A.W. Thomas, Phys. Rev. D **60**, 034014 (1999).
[3] D.B. Leinweber, A.W. Thomas, K. Tsushima, and S.V. Wright, Phys. Rev. D **61**, 074502 (2000).
[4] D.B. Leinweber, A.W. Thomas, and S.V. Wright, Phys. Lett. B **482**, 109 (2000).
[5] E.J. Hackett-Jones, D.B. Leinweber, and A.W. Thomas, Phys. Lett. B **489**, 143 (2000).
[6] E.J. Hackett-Jones, D.B. Leinweber, and A.W. Thomas, Phys. Lett. B **494**, 89 (2000).
[7] D.B. Leinweber, A.W. Thomas, and R.D. Young, Phys. Rev. Lett. **86**, 5011 (2001).
[8] W. Detmold, W. Melnitchouk, J.W. Negele, D.B. Renner, and A.W. Thomas, Phys. Rev. Lett. **87**, 172001 (2001).
[9] D.B. Leinweber, A.W. Thomas, K. Tsushima, and S.V. Wright, Phys. Rev. D **64**, 094502 (2001).
[10] W. Detmold, D.B. Leinweber, W. Melnitchouk, A.W. Thomas, and S.V. Wright, Pramana **57**, 251 (2001).
[11] R.D. Young, D.B. Leinweber, A.W. Thomas, and S.V. Wright, Phys. Rev. D **66**, 094507 (2002).
[12] S.V. Wright, D.B. Leinweber, and A.W. Thomas, Nucl. Phys. B (Proc. Suppl.) **119**, 236 (2003).
[13] R.D. Young *et al.*, Prog. Part. Nucl. Phys. **50**, 399 (2003).
[14] D.B. Leinweber, A.W. Thomas, and R.D. Young, hep-lat/0302020.
[15] I.C. Cloet, D.B. Leinweber, and A.W. Thomas, Phys. Lett. B **563**, 157 (2003).
[16] C. Bernard, S. Hashimoto, D.B. Leinweber, P. Lepage, E. Pallante, S.R. Sharpe, and H. Wittig, Nucl. Phys. B (Proc. Suppl.) **119**, 170 (2003).
[17] M. Luscher, S. Sint, R. Sommer, and P. Weisz, Nucl. Phys. **B478**, 365 (1996); M. Luscher, S. Sint, R. Sommer, P. Weisz, and U. Wolff, *ibid.* **B491**, 323 (1997); **B491**, 344 (1997).
[18] CSSM Lattice Collaboration, J.M. Zanotti *et al.*, Phys. Rev. D **65**, 074507 (2002).
[19] R. Narayanan and H. Neuberger, Phys. Lett. B **302**, 62 (1993); Nucl. Phys. **B412**, 574 (1994); Phys. Rev. Lett. **71**, 3251 (1993); Nucl. Phys. **B443**, 305 (1995).
[20] R.G. Edwards, U.M. Heller, and T.R. Klassen, Phys. Rev. Lett. **80**, 3448 (1998).
[21] D.B. Leinweber *et al.*, Eur. Phys. J. A **18**, 247 (2003).
[22] S.J. Dong, F.X. Lee, K.F. Liu, and J.B. Zhang, Phys. Rev. Lett. **85**, 5051 (2000).
[23] J.F. Donoghue, B.R. Holstein, and B. Borasoy, Phys. Rev. D **59**, 036002 (1999).
[24] S.R. Sharpe, Phys. Rev. D **46**, 3146 (1992); **41**, 3233 (1990).
[25] C.W. Bernard and M.F. Golterman, Phys. Rev. D **46**, 853 (1992).
[26] J.N. Labrenz and S.R. Sharpe, Phys. Rev. D **54**, 4595 (1996).
[27] D.B. Leinweber, Nucl. Phys. B (Proc. Suppl.) **109**, 45 (2002).
[28] M.J. Savage, Nucl. Phys. **A700**, 359 (2002).
[29] J.W. Chen and M.J. Savage, Phys. Rev. D **65**, 094001 (2002).
[30] S.J. Dong, K.F. Liu, and A.G. Williams, Phys. Rev. D **58**, 074504 (1998).
[31] Kentucky Field Theory Collaboration, N. Mathur and S.J. Dong, Nucl. Phys. B (Proc. Suppl.) **94**, 311 (2001).
[32] W. Wilcox, Nucl. Phys. B (Proc. Suppl.) **94**, 319 (2001).
[33] R. Lewis, W. Wilcox, and R.M. Woloshyn, Phys. Rev. D **67**, 013003 (2003); Nucl. Phys. B (Proc. Suppl.) **119**, 404 (2003).
[34] E. Jenkins *et al.*, Phys. Lett. B **302**, 482 (1993); **388**, 866(E) (1993).

[35] D.B. Leinweber, R.M. Woloshyn, and T. Draper, Phys. Rev. D **43**, 1659 (1991).
[36] D.B. Leinweber, T. Draper, and R.M. Woloshyn, Phys. Rev. D **46**, 3067 (1992).
[37] D.B. Leinweber, T. Draper, and R.M. Woloshyn, Phys. Rev. D **48**, 2230 (1993).
[38] D.B. Leinweber, Phys. Rev. D **47**, 5096 (1993).
[39] D.B. Leinweber, Phys. Rev. D **53**, 5115 (1996).
[40] D.B. Leinweber and A.W. Thomas, Phys. Rev. D **62**, 074505 (2000).
[41] SAMPLE Collaboration, R. Hasty *et al.*, Science **290**, 2117 (2000).
[42] HAPPEX Collaboration, K.A. Aniol *et al.*, Phys. Lett. B **509**, 211 (2001).
[43] The A4 Collaboration at MAMI and the G0 Collaboration at Jefferson Lab have experiments planned.
[44] E. Jenkins and A.V. Manohar, Phys. Lett. B **259**, 353 (1991).
[45] T.A. Rijken, V.G. Stoks, and Y. Yamamoto, Phys. Rev. C **59**, 21 (1999).
[46] M.F.L. Golterman, Acta Phys. Pol. B **25**, 1731 (1994).
[47] Y. Kuramashi, M. Fukugita, H. Mino, M. Okawa, and A. Ukawa, Phys. Rev. Lett. **72**, 3448 (1994).
[48] R. D. Young, D. B. Leinweber, and A. W. Thomas, in preparation.
[49] S.R. Sharpe and N. Shoresh, Phys. Rev. D **64**, 114510 (2001).